

# Great Himalayan earthquakes and the Tibetan plateau

Nicole Feld<sup>1</sup> & Roger Bilham<sup>1</sup>

**It has been assumed that Himalayan earthquakes are driven by the release of compressional strain accumulating close to the Greater Himalaya. However, elastic models of the Indo-Asian collision using recently imaged subsurface interface geometries suggest that a substantial fraction of the southernmost 500 kilometres of the Tibetan plateau participates in driving great ruptures. We show here that this Tibetan reservoir of elastic strain energy is drained in proportion to Himalayan rupture length, and that the consequent growth of slip and magnitude with rupture area, when compared to data from recent earthquakes, can be used to infer a ~500-year renewal time for these events. The elastic models also illuminate two puzzling features of plate boundary seismicity: how great earthquakes can re-rupture regions that have already ruptured in recent smaller earthquakes and how mega-earthquakes with greater than 20 metres slip may occur at millennia-long intervals, driven by residual strain following many centuries of smaller earthquakes.**

Approximately one-half of India's  $36\text{--}40\text{ mm yr}^{-1}$  northward motion is absorbed by convergence of the Himalaya, one-third in contraction of the Tibetan plateau, and the remainder is distributed between Tibet and Mongolia<sup>1,2</sup>. An important goal in Himalayan studies in the past decade has been to refine the Himalayan convergence rate, because this is responsible for the productivity of Himalayan earthquakes. It was anticipated that the uncertainty in the initial rate<sup>3</sup> would steadily decrease as more GPS (Global Positioning System) data became available. Although observed velocity uncertainties have decreased as expected, calculated convergence velocities range from  $14$  to  $20\text{ mm yr}^{-1}$  (Table 1), with a preferred rate in central and eastern Nepal of  $19 \pm 2.5\text{ mm yr}^{-1}$  (ref. 4). In Supplementary Information we present additional GPS data from 16 points between  $83^\circ\text{E}$  and  $87^\circ\text{E}$  (Fig. 1) measured between 1991 and 2004 that further constrain the Himalayan convergence velocity.

We attempted initially to emulate the observed velocity field, as in previous studies, as the product of uniform creep on a planar dislocation beneath the plateau. This yielded a slip rate of  $17 \pm 1\text{ mm yr}^{-1}$  on a  $6^\circ$ , N12E dipping dislocation starting at 18 km depth, consistent with earlier results (Fig. 2), but we noted that our result (and its uncertainty) was influenced by the retention or rejection of GPS data 100–300 km north of the Himalayan foothills. No abrupt transition in surface velocity distinguishes the strain field above the process zone of Himalayan seismicity from that of the Tibetan plateau, whose  $17 \times 10^{-9}$  strain  $\text{yr}^{-1}$  north-northeast-directed contraction and east-southeast-directed extension have been interpreted as resulting from dynamic processes responsible for inelastic, permanent deformation of the plateau<sup>5</sup>. As the inclusion of more northerly GPS points biases interpretations of Himalayan convergence velocities to higher values, we adopted a different approach, where the Himalayan and Tibetan velocity fields are considered the surface manifestation of a single deformational process related to the slip of India beneath the plateau. Our study indicates that although the region of elastic strain accumulation and release is much broader than hitherto supposed, less than one-fifth of the strain currently accumulating in the southern 500 km of the plateau participates in the earthquake cycle.

## A boundary element model for interseismic deformation

We assume that frictionless aseismic slip occurs between the descending Indian plate and the overlying Tibetan plateau in an elastic half-space. We simplified the Himalayan arc as a straight line, but used a receiver-function image of the descending Indian plate<sup>6</sup> as a 'cylindrical' subsurface starting geometry at its southern edge. We emulate this subsurface geometry with 14 contiguous, parallel, freely slipping boundary elements, with 64 elements along-strike<sup>7</sup> extending 500 km north of the Himalaya (Fig. 2). Element dimensions are 50 km along-strike, and 2 km wide near the Himalaya increasing to 180 km in the north. We imposed an appropriate convergence velocity on the northernmost element and an overall strain contraction rate at N10E to drive the model (see Supplementary Information). We then calculated the displacement on each segment needed to minimize stress in its vicinity<sup>7–9</sup> in response to these imposed loading conditions, and compared the resulting surface velocities with the observed horizontal and vertical velocities in the Himalaya and southern Tibet.

Although we tested several different northern boundaries for the model, we ultimately selected a northernmost driving segment whose southern edge lies close to where the plateau's surface converges with the Indian plate at a velocity of  $21\text{ mm yr}^{-1}$ . This occurs ~550 km north of the frontal thrusts, near the Karakorum/Jiali fault system. The Himalaya advance over India at  $14\text{ mm yr}^{-1}$  (refs 10 and 11) to  $21\text{ mm yr}^{-1}$  (ref. 12), and the simplest assumption is that to sustain the highest rates of advance, at least 550 km of the southern plateau must participate in driving the Himalaya's southward advance. We determined that a surface convergence velocity of  $21\text{ mm yr}^{-1}$  550 km north of the frontal thrusts can be obtained by imposing a background strain of  $-4.8 \times 10^{-8}\text{ yr}^{-1}$ , and by driving the boundary element model with uniform slip of  $25\text{ mm yr}^{-1}$  on a wide horizontal synthetic thrust fault 49 km below the plateau surface, whose southern edge lies 594 km north of the frontal thrusts. The driven dislocation is sufficiently far north to not introduce local gradients in the region of interest. To match the surface velocity field to GPS observations southward, we found it necessary to introduce minor adjustments to the depth and dip of the descending Indian plate near the transition from aseismic to seismic slip. Starting from the 'locking line' of our planar, uniform-slip model<sup>3</sup>, the best fit was obtained by

<sup>1</sup>CIRES and Department of Geological Sciences, University of Colorado, Boulder, Colorado 80309, USA.

**Table 1 | Himalayan convergence rates**

Interval	Slip rate (mm yr <sup>-1</sup> )	Locking depth (km)	Dip (°)	Location	Source
1991–1995	20 ± 2 (18 ± 2*)	20 ± 4	4 ± 4	81–88° Nepal	Ref. 3
1991–1997	20 ± 1	15	3	Eastern Nepal	Ref. 36
	21 ± 2	25	4.5	Western Nepal	
	20 ± 1 (18 ± 2*)	18	5	Combined	
1991–1997	17.4 ± 0.7	9	0	Eastern Nepal	Ref. 37
	16.3 ± 0.4	12	1	Western Nepal	
1995–2000	19–20	17–21	9–10	Central Nepal	Ref. 38
	19	20–21	9–10	Western Nepal	
1995–2000	14 ± 1	15	6	Northwest India	Ref. 39
1997–2000	19 ± 3*	ND	ND	Ladakh	Ref. 40
1991–2000	17 ± 0.9	18.3	9.5	West Himalaya	Ref. 41
	12.2 ± 0.4	14.3	2.5	Central Himalaya	
	17.5–19	20.3	3	Eastern Himalaya	
1992–2004	19 ± 2.5	20.4	10.3	Central Nepal	Ref. 4 This study (planar models) <sup>42</sup>
1992–2004	17 ± 2	18	9	Eastern Nepal	
	19 ± 3	18	6	Central Nepal	
	17 ± 1	18	9	Combined	
	21 ± 1.5	ND	ND	Central Nepal	
Holocene	≥14 ± 4	ND	ND	Kumaon Himal	Ref. 11
Holocene	≥12 ± 3	ND	ND	NW India	
Late Cenozoic	10–15*	ND	ND	73–87° Himalaya	Ref. 10
Late Cenozoic	18 ± 7*	ND	ND	73–87° Himalaya	Ref. 16

\* Observed surface convergence rate, rather than estimated slip rate on dislocation. Current convergence rates are based largely on planar elastic dislocation models that derive a subsurface slip rate to emulate the surface velocities of GPS data. ND, not determined.

extending the region of aseismic slip 7.5 km further south, by reducing its depth from 18 to 15 km, and by increasing its dip from 9° to 22° N. These geometrical adjustments are permitted by current uncertainties in the geometry of the interface<sup>6</sup>, and the probable presence of a structural ramp beneath the Greater Himalaya. A feature of these elastic models is that they predict a broad region where the basal slip-velocity reduces to zero at the tip of the dislocation beneath and south of the Greater Himalaya. Finite element models that have included rock rheology also report a wide region where slip reduces to zero<sup>13</sup>. The termination of interseismic slip 83 km north of the frontal thrusts reduces the width of Himalayan ruptures from previous estimates (90–110 km) unless additional coseismic slip

extends downdip during earthquakes into the region of interseismic slip. Downdip slip here is essential either as coseismic slip or afterslip to eliminate the accumulation of a permanent slip deficit. We later compute its numerical value and spatial distribution.

The dip required by the model beneath the Greater Himalaya is in good agreement with the average dip of moderate earthquakes occurring there<sup>14–16</sup>. Whereas the fit to the horizontal GPS data and vertical levelling data<sup>17</sup> is satisfactory, predicted vertical deformation is broader than that associated with planar, uniform slip models<sup>3</sup>. Vertical GPS data in southern Tibet are insufficiently precise at present to test the predicted width of this vertical uplift<sup>18,19</sup>. In contrast to the sensitivity of the model to the geometry of the descending Indian plate at depths shallower than 20 km, tests showed that the misfit in central Tibet is largely insensitive to the depth of the interface further north.

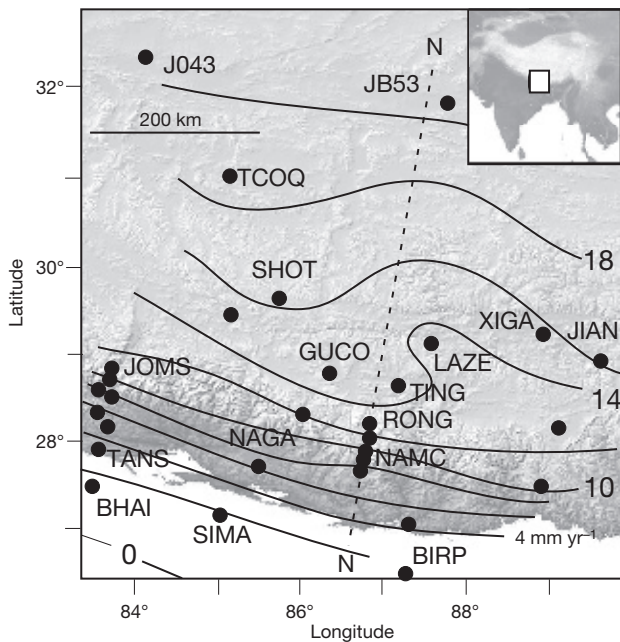


**Figure 1 | The southern Tibetan plateau and Himalaya.** Filled circles, GPS points; contours, the N10E GPS velocity field relative to India fixed; dashed line, the N10E velocity profile shown in Fig. 2. Inset, location of study area.

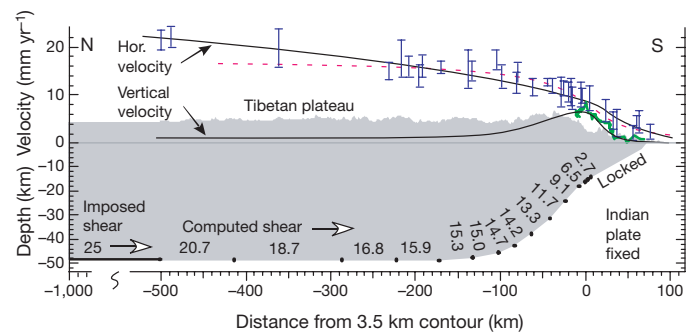


**Figure 2 | Observed and synthetic present-day velocity fields for the southern Tibetan plateau.** Observed fields are shown blue (horizontal GPS) and green (spirit-levelling<sup>17</sup>); synthetic fields are shown black; error bars are 1σ. Calculated interseismic segment velocities (mm yr<sup>-1</sup>) and the geometry of freely slipping boundary elements are indicated at the base of plateau. The model is driven by a thrust fault in the north at 25 mm yr<sup>-1</sup> (sense of shear indicated by arrow), and a background strain contraction rate of 4.8 × 10<sup>-8</sup> yr<sup>-1</sup> (corresponding to the mean strain rate between -500 km and the locking line). Dots indicate segment boundaries. The red dashed line shows the predicted velocity from the best-fitting planar dislocation model (see Supplementary Information). The grey shaded region represents the subsurface geometry and topography of the plateau.

**Table 2 | Himalayan earthquake magnitude and slip versus rupture length**

Length (km)	10	20	40	60	80	100	150	200	300	400	600	1200	2000
<i>M<sub>w</sub> restrained</i>	6.71	6.95	7.41	7.71	7.99	8.1	8.26	8.37	8.49	8.59	8.71	8.86	9.06
<i>Max. slip (m)</i>	3.41	3.81	4.55	5.64	6.98	7.78	8.76	9.05	9.12	9.11	9.11	9.12	9.12
<i>Ave slip (m)</i>	2.12	2.43	3.02	3.75	4.63	5.31	6.31	6.8	7.15	7.36	7.44	7.48	7.48
<i>M<sub>w</sub> unrestrained</i>	6.72	6.96	7.42	7.77	8.05	8.18	8.36	8.5	8.66	8.77	8.9	9.13	9.28
<i>Max slip (m)</i>	3.42	3.85	4.74	7.43	9.12	10.86	13.14	15.31	17.42	18.57	19.72	20.91	21.05
<i>Ave. slip (m)</i>	2.24	2.47	3.11	4.55	5.5	6.75	8.51	10.34	12.07	13.05	13.86	15.04	15.41
Max. 0–50 km N	0.01	0.05	0.11	1.12	1.57	2.29	3.65	5.69	8.22	9.83	11.52	13.2	13.4
Max. 50–200 km N	0	0.03	0.06	0.31	0.49	0.74	1.24	2.1	3.43	4.5	5.86	7.47	7.68

Calculations for 1,000 yr of Indo/Asian convergence at current rate. A halving in strain accumulation time (500 yr), consistent with ruptures in the past century (Fig. 4), halves the potential slip and reduces magnitudes by 0.2  $M_w$  units. For ruptures where length  $L \geq 80$  km, width  $w$  is 83 km. For ruptures where  $L < 80$  km, areas are equidimensional. The first three rows in italics indicate Himalayan slip assuming that there is no coseismic slip beneath the plateau (restrained slip). The remaining five rows indicate coseismic or postseismic slip assuming that the plateau responds to the sudden southward shift in boundary conditions following Himalayan earthquakes (unrestrained slip). Unrestrained  $M_w$  magnitudes in row 4 are calculated assuming all slip is seismic. These end-member solutions form the upper and lower bounds of areas plotted in Fig. 4a and b. Maximum unrestrained trans-Himalayan coseismic displacements 0–50 km north of each rupture, and 50–200 km north of each rupture, are indicated in the last two rows.

### Rupture length, earthquake magnitude and recurrence interval

We next examined the efficiency with which distributed strain stored within the southern plateau can be delivered to Himalayan earthquakes. Assuming that rupture occurs between the southernmost tip of interseismic slip beneath the plateau and the frontal thrusts, and that the slip is frictionless, the length of Himalayan ruptures determines the slip and consequently the magnitude of the earthquake. For example, if interseismic displacements were to accumulate in our model for 1,000 yr at present rates, the Himalaya would slip 21 m, were it to do so in a single massive earthquake. Assuming a rupture width of 83 km and length of 1,800 km, the moment magnitude of this improbably large earthquake would be  $M_w = 9.2$  (Table 2). A 500-yr recurrence interval, however, would result in half the slip and a  $M_w = 9.0$  earthquake. To calculate the slip on shorter rupture lengths, we incremented the slip velocities of our best-fitting interseismic boundary element model by 1,000 yr, and emulated an earthquake rupture by adding a freely slipping rectangular dislocation to its southernmost edge (Fig. 3). This additional rectangular region represents rupture of the Himalayan decollement, and was modelled as a  $5 \times 10$  matrix of freely slipping elements, whose integrated slip and area were used to calculate  $M_w$ . In these synthetic earthquakes, we determined both the maximum and mean slip on the earthquake rupture, as well as the change of slip and strain beneath southern Tibet resulting from the occurrence of each Himalayan rupture (Table 2).

Two end-member models were considered. In the first, we calculate Himalayan slip assuming that no slip beneath the plateau accompanies rupture—that is, coseismic slip at the northern edge of the earthquake ceases abruptly at the southern edge of the region of aseismic slip. In the second, we calculate the combined change in slip on the earthquake rupture and beneath the plateau—that is, the northern edge of the earthquake rupture is unrestrained and is driven by strain relaxation in the southern plateau. This unrestrained additional slip more than doubles the maximum slip available to drive the

frontal thrusts. This downdip slip presumably occurs as afterslip resulting in rate changes following rupture<sup>20</sup>; however, the 6 June 1505 earthquake<sup>21</sup> with its inferred 600-km-long rupture length was accompanied by substantial accelerations in southern Tibet, consistent with some of this downdip slip occurring co-seismically. Our results (Table 2 and Fig. 4) demonstrate that, as expected, for earthquakes with rupture lengths shorter than the width of the Himalaya, magnitude scales with area, whereas those longer than 90 km scale with length. Similar observed, and synthetic, scaling relations have been reported for transform faults<sup>22–24</sup>. Ruptures shorter than ~150 km leave strain in southern Tibet largely untapped, whereas longer ruptures drain this energy, resulting in larger slip both in the region of coseismic rupture and as increased slip downdip from the rupture beneath the plateau (Figs 4, 5).

The renewal time for Himalayan earthquakes is unknown, because no large earthquakes have recurred repeatedly in the historical record. The slip released in recent earthquakes compared to present-day Himalayan convergence rates suggests that the renewal time is of the order of 300–1,000 yr. This estimate can be improved using the synthetic scaling law depicted in Fig. 4, by selecting a renewal time consistent with  $M_w$  versus rupture-length data from recent earthquakes. Only for the 2005 Kashmir earthquake are slip and geometry well constrained, but the convergence rate in western Kashmir is lower, and the geometry of its rupture steeper, than for earthquakes we consider here. Such data as are available are consistent with a recurrence interval of ~500 yr, and suggest that recent ruptures best fit the restrained rupture model (the lower bound of the envelopes in Fig. 4).

Whereas the maximum slip in recent earthquakes is consistent with maximum slip predicted in synthetic earthquakes with a 500-yr return time, trench excavations of surface ruptures of medieval earthquakes record slip that would require  $\geq 1,000$  yr of strain accumulation<sup>25,26</sup>. Minimum rupture lengths only are available for these earthquakes, but our models imply that they ruptured much longer fault planes than

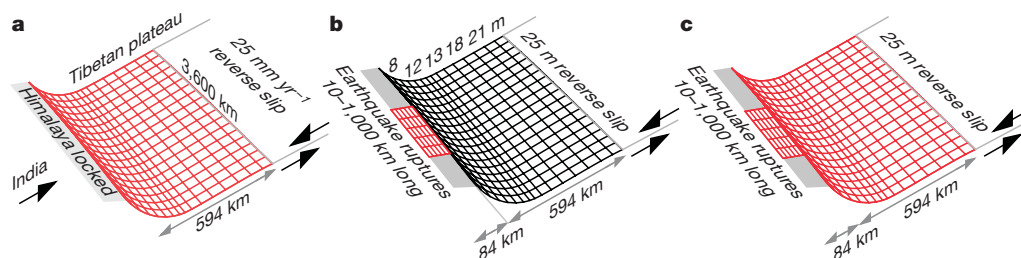


**Figure 3 | Boundary element meshes used to derive synthetic slip.** Red elements slip freely in response to imposed slip. **a**, Interseismic velocities calculated by driving 3,450 freely slipping elements with southerly geometry adjusted to emulate observed surface GPS data. **b**, Restrained coseismic slip. Velocities from **a** are used to derive displacements whose resulting strain field drives ruptures of different lengths in the Himalaya (Table 2). The

displacements shown correspond to a millennium of slip at current rates. **c**, Slip beneath the Himalaya changes the boundary conditions in the southern plateau, causing additional slip both on the main rupture and beneath the plateau. When fully expressed, this unrestrained slip represents maximum afterslip (Table 2 and Fig. 4).

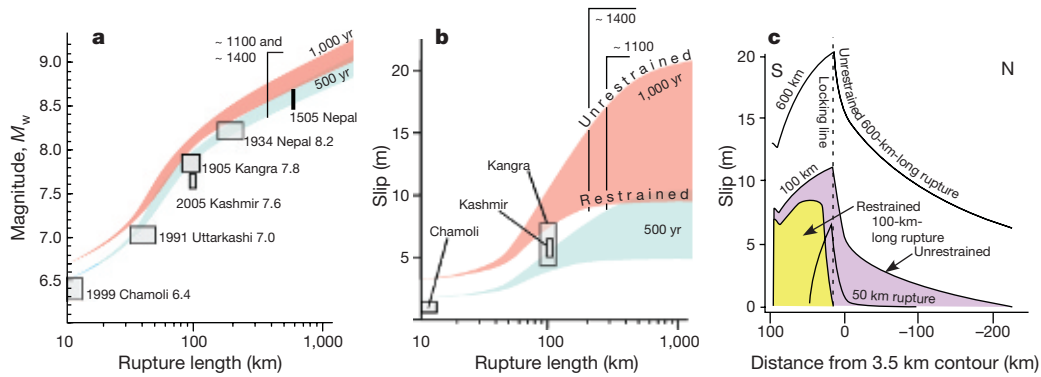


**Figure 4 | Synthetic scaling laws for Himalayan earthquakes.** Pink areas in **a** and **b** represent predictions for 1,000-yr intervals between earthquakes; blue areas represent predictions for 500 yr. The upper and lower bounds of these shaded areas correspond to restrained coseismic slip, and unrestrained slip, respectively. Restrained slip occurs coseismically when the interface below the plateau remains locked during the earthquake. **a**,  $M_w$  versus rupture-length curves suggest observed earthquakes recur after  $\sim 500$ -yr intervals. **b**, Envelopes indicate minimum slip (no plateau afterslip) and maximum slip (full strain release) for Himalayan ruptures. Maximum slip in medieval earthquakes requires  $>1,000$  yr strain accumulation intervals.

Open boxes are minimum estimates for historical ruptures ( $>300$  km for about AD 1100 (ref. 26) and  $>200$  km about AD 1400 (ref. 25)). The eastern Nepal earthquake of 6 June 1505 is believed to have ruptured 600 km along the arc<sup>21</sup> and its recurrence now would release  $\sim 9$  m of slip in a  $M_w \approx 8.6$  earthquake (vertical bar in **a**). **c**, Maximum fault slip versus north/south distance as a function of rupture length. Yellow indicates restrained coseismic slip for a 100-km-long rupture (no slip north of the locking line); violet indicates complete unrestrained strain release (frictionless slip beneath the plateau). The kink in the south is caused by the surface rupture of the steeply dipping Main Boundary Fault.

recent earthquakes (Table 2). A possible explanation for these observations of large slip is that they are amplified locally by the dynamics of rupture<sup>23,27</sup>, but it is more probable that long ruptures (megaquakes) at infrequent intervals are essential to occasionally reduce residual

elastic strain accumulating in the southern plateau that has been left by previous smaller earthquakes. The past 500 yr, for example, are characterized by earthquakes with rupture lengths  $<300$  km that have inefficiently reduced cumulative elastic strain.

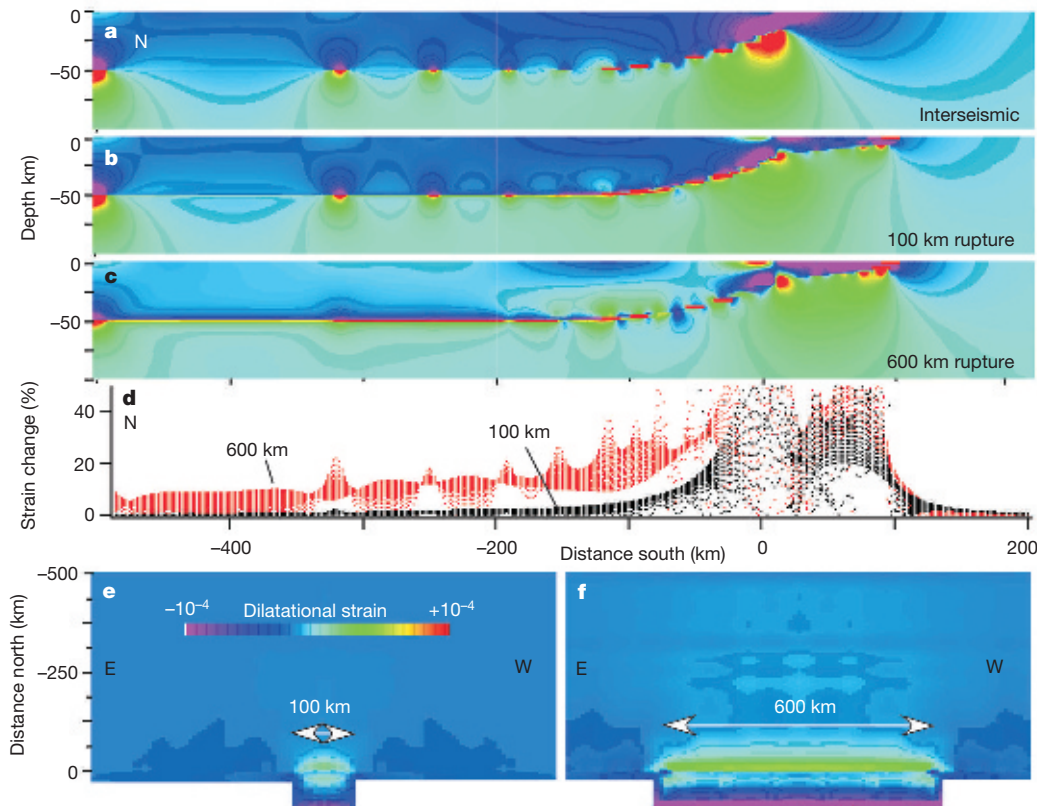


**Figure 5 | Unrestrained strain changes in the southern Tibetan plateau generated by synthetic earthquakes with 100-km-long ( $8 < M_w < 8.2$ ) and 600-km-long ( $8.4 < M_w < 8.6$ ) ruptures.** Shown are cross-sections (**a–d**) and map views (**e, f**). **a**, Pre-seismic dilatational strain associated with 1,000 yr of strain accumulation at the current rate. **b, c**, Coseismic changes caused by earthquakes with 100-km (**b**) and 600 km (**c**) rupture lengths (**e** and **f** are respective map views of surface strain changes). **d**, Calculated

percentage strain changes in the uppermost 40 km of the plateau for these two lengths of rupture. Cusps and strain concentrations in each panel are artefacts caused by junctions between boundary elements (see Fig. 2). Cross-sections **a–c** sample the centre of each rupture, but **d** samples all points shallower than 45 km throughout a  $\pm 500$ -km east–west length of the southern plateau. Colour coding for dilatational strain in **a–c** and **f** shown in **e**.

### Seismic gaps versus failures in seismic gap theory

We note that our inferred renewal time applies to earthquakes of all magnitudes, which is an apparent departure from the predictions of seismic gap theory. Seismic gaps are unruptured segments of a plate boundary that slip eventually in great earthquakes. Their rupture results in an earthquake whose magnitude is characteristically proportional to the cumulative plate boundary displacement since their previous rupture. Our models suggest that once a critical strain has been attained, its release by a  $M_w < 7$  or a  $M_w > 9$  earthquake depends only on the length of the rupture, the growth of which in the Himalaya is presumably impeded by the presence of along-arc asperities<sup>28</sup>. Insufficient earthquakes are known in the Himalaya to determine whether successive earthquakes rupture similar areas.

A second apparent departure from seismic gap theory is that our model demonstrates that a major earthquake can be followed by a great earthquake in the same location, sooner than anticipated from considerations of renewal time from plate convergence rates. Such behaviour is manifest in other convergence zones: in Chile<sup>29</sup> and in the 2004 Sumatra/Andaman earthquake<sup>30</sup>. Himalayan  $M_w < 8$  earthquakes drain negligible elastic energy from southern Tibet compared to those where  $M_w > 8$ . This can explain, for example, why the 1833  $M_w = 7.8$  Nepal earthquake was followed by the 1934  $M_w = 8.2$  Bihar/Nepal earthquake in approximately the same area after only 101 yr (ref. 31). It also implies that the 1905 Kangra earthquake region, previously considered a region relieved from an imminent damaging earthquake, could today host one of larger magnitude<sup>32</sup>.

That the elastic cycle accompanying Himalayan earthquakes must modulate the stresses that drive the long term flow behaviour of the plateau has never been questioned, but its influence in the southern-most 500 km of the plateau is unexpected. The elastic model we propose for the Tibetan plateau is a one-parameter model, driven by hypothetical reverse slip less than 500 km north of the Himalaya. This remote driving condition is not a unique requirement of the model, and similar results can be obtained using more northerly boundary conditions driven at higher rates, indicating that our conclusions are unaffected by elastic conditions in central and northern Tibet. Our traction-free lower boundary conditions at the base of the plateau are common to both dynamic<sup>33</sup> and kinematic models proposed for the Tibetan plateau<sup>34</sup>, but unlike previous studies that incorporate realistic subsurface interface geometry, we incorporate no depth-dependent rheology, nor rate-dependent friction laws. Although the models may be refined further, the implications for earthquake scaling laws in the Himalaya are unlikely to change significantly.

The dynamic deformation of the Tibetan plateau is driven by the same forces that drive earthquakes in the Himalaya, and it is thus of some interest to estimate what fraction of present day strain accumulation in the plateau participates in the elastic earthquake cycle. Accordingly, we calculated the percentage of elastic strain released in the uppermost 40 km on a 2-km three-dimensional grid spacing throughout the southern plateau (Fig. 5d). Strain changes exceed 40% within 120 km of the Himalayan front but fall rapidly northward. For 100-km- and 600-km-long ruptures, dilatational strain changes average less than 10% and 20%, respectively, hence most of the observed interseismic strain remains to drive the dynamics and kinematics of the plateau.

The absence of surface ruptures for nineteenth- and twentieth-century central Himalayan earthquakes<sup>35</sup> suggests that their rupture lengths may have been atypically short (<200 km), and their slip correspondingly low. According to our models, the lengths of ruptures in about 1100 and 1400, which did rupture the surface, may have exceeded 400 km, with moment magnitudes exceeding  $M_w = 8.6$ . A ~500-yr recurrence interval for Himalayan earthquakes suggests that the western Himalaya (last mega-event in about 1400), the central Himalayan seismic gap (1505) and eastern Nepal (1100) are now sufficiently mature to sustain renewed rupture, but that the large observed slips (>20 m) of the first and last of these may require

the elapse of a further five centuries before they repeat with equal severity.

Received 26 January; accepted 25 August 2006.

- DeMets, C., Gordon, R. G., Argus, D. F. & Stein, S. Effect of recent revisions to the geomagnetic reversal time scale on estimates of current plate motions. *Geophys. Res. Lett.* **21**, 2191–2194 (1994).
- Zhang, P. et al. Continuous deformation of the Tibetan Plateau from global positioning system data. *Geology* **32**, 809–812 (2004).
- Bilham, R., Larson, K., Freymueller, J., Project Idrivhim members. GPS measurements of present-day convergence across the Nepal Himalaya. *Nature* **386**, 61–64 (1997).
- Bettinelli, P. et al. Plate motion of India and interseismic strain in the Nepal Himalayan from GPS and DORIS measurements. *J. Geod.* doi:10.1007/s00190-006-0030-3 (published online 8 March, 2006).
- Houseman, G. & England, P. Crustal thickening versus lateral expulsion in the India-Asia continental collision. *J. Geophys. Res.* **98**, 12233–12249 (1993).
- Schulte-Pelkum, V. et al. Imaging the Indian Subcontinent beneath the Himalaya. *Nature* **435**, 1222–1225 (2005).
- Crouch, S. L. & Starfield, A. M. *Boundary Element Methods in Solid Mechanics* (Allen Unwin, London, 1983).
- Gomberg, J. & Ellis, M. Topography and tectonics of the central New Madrid seismic zone: Results of numerical experiments using a three-dimensional boundary-element program. *J. Geophys. Res.* **99**, 20299–20310 (1994).
- Okada, Y. Internal deformation due to shear and tensile faults in a half-space. *Bull. Seismol. Soc. Am.* **82**, 1018–1040 (1992).
- Lyon-Caen, H. & Molnar, P. Gravity anomalies, flexure of the Indian plate, and the structure, support and evolution of the Himalaya and Ganga Basin. *Tectonics* **4**, 513–538 (1985).
- Wesnousky, S. G., Kumar, S., Mohindra, R. & Thakur, V. C. Uplift and convergence along the Himalayan Frontal Thrust of India. *Tectonics* **18**, 967–976 (1999).
- Lave, J. & Avouac, J. P. Active folding of fluvial terraces across the Siwaliks Hills, Himalayas of central Nepal. *J. Geophys. Res.* **105**, 5735–5770 (2000).
- Cattin, R. & Avouac, J. P. Modelling mountain building, the seismic cycle in the Himalaya of Nepal. *J. Geophys. Res.* **105**, 13389–13407 (2000).
- Molnar, P. & Lyon-Caen, H. Fault plane solutions of earthquakes and active tectonics of the Tibetan Plateau and its margins. *Geophys. J. Int.* **99**, 123–153 (1989).
- Chen, W.-P. & Molnar, P. Seismic moments of major earthquakes and the average rate of slip in Central Asia. *J. Geophys. Res.* **82**, 2945–2969 (1977).
- Molnar, P. A review of geophysical constraints on the deep structure of the Tibetan Plateau, the Himalaya, and the Karakorum and their tectonic implications. *Phil. Trans. R. Soc. Lond. A* **326**, 33–88 (1988).
- Jackson, M. & Bilham, R. Constraints on Himalayan deformation inferred from vertical velocity fields in Nepal and Tibet. *J. Geophys. Res.* **99**, 13897–13912 (1994).
- Chen, J. Y. & Zhang, J. On the crustal movement in Quomolongma Feng and its adjacent area. *Acta Geophys. Sinica* **39**, 67–78 (1996).
- Xu, C., Jungnan Liu, W. J. & Chuang, S. GPS measurements of present day uplift in Southern Tibet. *Earth Planets Space* **52**, 735–739 (2000).
- Perfettini, H. & Avouac, J. P. Stress transfer and strain rate variations during the seismic cycle. *J. Geophys. Res.* **109**, doi:10.1029/2003JB002917 (2004).
- Ambraseys, N. & Jackson, D. A note on early earthquakes in northern India and southern Tibet. *Curr. Sci.* **84**, 570–582 (2003).
- Wells, D. L. & Coppersmith, K. L. New empirical relationships among magnitude, rupture width, rupture area, and surface displacement. *Bull. Seismol. Soc. Am.* **84**, 974–1002 (1994).
- Shaw, B. E. & Scholz, C. H. Slip-length scaling in large earthquakes: Observations and theory and implications for earthquake physics. *Geophys. Res. Lett.* **28**, 2995–2998 (2001).
- Bodin, P. & Bilham, R. 3-D geometry at transform plate boundaries: Implications for seismic rupture. *Geophys. Res. Lett.* **21**, 2523–2526 (1994).
- Kumar, S. et al. Paleoseismic evidence of great surface rupture earthquakes along the Indian Himalaya. *J. Geophys. Res.* **111**, B03304, doi:10.1029/2004JB003309 (2006).
- Lave, J. et al. Evidence for a great medieval earthquake (~1100 A.D.) in the Central Himalayas, Nepal. *Science* **307**, 1302–1305 (2005).
- Brune, J. N., Brown, S. & Johnson, P. A. Rupture mechanism and interface separation in foam rubber models of earthquakes: a possible solution to the heat flow paradox and the paradox of large overthrusts. *Tectonophysics* **218**, 59–67 (1993).
- Bollinger, L., Avouac, J. P., Cattin, R. & Pandey, M. R. Stress buildup in the Himalaya. *J. Geophys. Res.* **109**, doi:10.1029/2003JB002911 (2004).
- Cisternas, M. et al. Predecessors of the giant 1960 Chile earthquake. *Nature* **437**, 404–407 (2005).
- Bilham, R., Engdahl, E. R., Feldi, N. & Satyabala, S. P. Partial and complete rupture of the Indo-Andaman plate boundary 1847–2004. *Seismol. Res. Lett.* **76**, 299–311 (2005).
- Bilham, R. Earthquakes in India and the Himalaya: Tectonics, geodesy, and history. *Ann. Geophys.* **74**, 839–858 (2004).
- Bilham, R. & Wallace, K. Future  $M_w > 8$  earthquakes in the Himalaya: Implications from the 26 Dec 2004  $M_w = 9.0$  earthquake on India's eastern plate margin. *Geol. Surv. India Spec. Publ.* **85**, 1–14 (2005).

33. England, P. & Molnar, P. Active deformation of Asia: From kinematics to dynamics. *Science* **278**, 647–650 (1997).
34. Tapponnier, P. *et al.* Oblique stepwise rise and growth of the Tibet Plateau. *Science* **294**, 1671–1677 (2001).
35. Bilham, R. & Ambraseys, N. Apparent Himalayan slip deficit from the summation of seismic moments for Himalayan earthquakes, 1500–2000. *Curr. Sci.* **88**, 1658–1663 (2005).
36. Larson, K., Burgmann, R., Bilham, R. & Freymueller, J. Kinematics of the India-Eurasia collision zone from GPS measurements. *J. Geophys. Res.* **104**, 1077–1093 (1999).
37. Burgmann, R., Larson, K. & Bilham, R. Model inversion of GPS and leveling measurements across the Himalaya: Implications for earthquake hazards and future geodetic networks. *Himal. Geol.* **20**, 59–72 (1999).
38. Jouanne, F. *et al.* Current shortening across the Himalayas of Nepal. *Geophys. J. Int.* **157**, 1–14 (2004).
39. Banerjee, P. & Burgmann, R. Convergence across the northwest Himalaya from GPS measurements. *Geophys. Res. Lett.* **29**, 31–34 (2002).
40. Jade, S. *et al.* GPS measurements from the Ladakh Himalaya, India: Preliminary tests of plate-like or continuous deformation in Tibet. *Geol. Soc. Am. Bull.* **116**, 1385–1391 (2004).
41. Chen, Q. *et al.* Spatially variable extension in southern Tibet based on GPS measurements. *J. Geophys. Res.* **109**, B09401, doi:10.1029/2002JB002350 (2004).
42. Feldl, N. *Crustal Deformation Across the Himalaya of Central and Eastern Nepal*. MSc thesis, Univ. Colorado (2005).

**Supplementary Information** is linked to the online version of the paper at [www.nature.com/nature](http://www.nature.com/nature).

**Acknowledgements** Discussions with P. Bodin, J. Gombert, G. King, P. Molnar and W. Szeliga, and written comments from S. Wesnousky, J.-P. Avouac and J. Freymueller, have improved the manuscript. This paper is based upon work supported by the National Science Foundation.

**Author Contributions** The 2003/4 GPS observations in Nepal were conducted by N.F. and R.B., and the planar dislocation models presented here formed the focus of N.F.'s MSc thesis at the University of Colorado.

**Author Information** Raw GPS data are available from UNAVCO (<http://www.unavco.org/>). Reprints and permissions information is available at [www.nature.com/reprints](http://www.nature.com/reprints). The authors declare no competing financial interests. Correspondence and requests for materials should be addressed to R.B. ([bilham@colorado.edu](mailto:bilham@colorado.edu).)

# Supplementary information

From the following article:

[Great Himalayan earthquakes and the Tibetan plateau](#)

Nicole Feldl & Roger Bilham

*Nature* **444**, 165-170(9 November 2006)

doi:10.1038/nature05199

## [Download plugins and applications](#)

### Supplementary Information

This file contains Supplementary Figures, Supplementary Data and Supplementary Results. This file also includes a brief description of files used as input to the boundary element program 3D-def coded by Ellis and Gomberg. Sample files are attached ready to be input into the code, which is provided as a .tar file for operation on an Apple unix terminal.

[Download PDF file \(780KB\)](#)

### Supplementary Data 1

The input file 300map is for 300-km-long unrestrained rupture with a total of 29 planes each divided into 50 segments along strike. The first two planes are a rupture fronting the Himalaya divided into five segments along-strike and five elements down-dip, the first being a steep ramp and the second a gently dipping decollement. It outputs a map view of the surface strain (suffix .m300) and a segment displacement listing in a north-south line through the center of the rupture. Columns 2 and 3 after the line that starts "for each plane" indicate the start points (distance and depth) of each segment, and columns 5 and 9 indicate the length and dip respectively. The along-strike length of the interseismic driving condition is 3600 km and in this model each segment width is 56.25 km. All elements are freely-slipping (code 12) except the most northerly plane and last listed plane (segment 30 is code 10) which drives the system at 25 mm/year, or in the case of coseismic rupture with an imposed displacement of 25 m. The first two planes specified are the Himalayan rupture, the first plane representing a 45° north-dipping 5.7-km-long ramp-thrust that cuts the surface. If these planes are removed and the number of planes reduced from 17 to 15 in line 2, the file can be used to calculate pre-seismic displacements or interseismic velocities. Strain and displacement changes accompanying rupture can then be obtained by subtracting the two output matrices.

[Download Text file \(89KB\)](#)

### Supplementary Data 2

This is an input file to 3ddef (see details below) that produces a strain cross section with the suffix .i400. Length east west is 1700 km, width N/S is 500 km, and it has fewer segments to speed computation. Sixty four along-strike segments are placed beneath the southern plateau, reducing to thirty-two 72 km north of the locking line. As before the rupture consists of two planes each with 25 segments.

[Download Text file \(47KB\)](#)

### Supplementary Data 3

This is a tar file that when unpacked produces a folder with 14 files including the executable

3ddef program compiled in Fortran 91 which will run in the terminal mode on Apple computers. See the readme.first for a message from Ellis and Gomberg. The README file from Walter Szeliga lists the changes made to prevent matrix arrays from overflowing. Place the input files section400 or 300map in the folder 3ddef once it has been de-compressed. To run the program from "Terminal", change the directory to 3ddef [cd desktop/3ddef] then type ./3d and enter the appropriately named input file when prompted. The program will run in the background, but will be faster if no other tasks are running.

[Download tar \(240KB\)](#)

## Supplementary materials: "Great Himalayan earthquakes and the Tibetan Plateau"

Nicole Feldl and Roger Bilham

We provide details of GPS data acquisition and analysis from 1991-2004, plus information on modeling these GPS data first as slip on a planar fault with uniform slip and dip beneath southern Tibet, and then as slip on a geometrically complex surface driven from >500 km to the north. We describe typical 3d-def boundary element input files of the form we used in our calculations. These files are named *b150section* and *m300map*. A version of the 3d deformation program<sup>22-24</sup> compiled in Fortran 91 is provided as an additional supplement (*3ddef.tar*).

### Data from Nepal

Since first submission of this article a rigorous analysis of GPS and DORIS points in Nepal has been published<sup>1</sup>. We here report our analysis of a subset of those GPS points and additional points in eastern and central Nepal that were measured in 2003-2004 and were not included in that analysis. Inasmuch as our solutions agree within the respective uncertainties, our data are presented to complement this previous analysis and to provide a starting point for the models we later discuss. The most northerly of these sixteen points are JOMS in the Kali Gandaki valley and KPFB in the Khumbu valley, a few kilometers west of Everest (see Figure 1 in main text). Some of these points were first measured in 1991, although pre-1992 data were discarded due to reference frame errors induced by the absence of a global GPS tracking network and unavailability of precise satellite orbits. Measurements were made in campaign style surveys, supplemented by brief segments of continuous tracking at four sites. The 13 year span of raw GPS data (Table 1) were analyzed using Bernese 4.2 software<sup>2</sup> with continuous station data from the IGS network to generate a global solution in ITRF2000: 36-37 IGS stations with global coverage were included in the 1998-2004 solution, 31-32 for 1996-1997, 27 for 1995, and 12 for 1992. Precise CODE final satellite orbits and antenna phase-center offsets were included in the analysis. Receiver clock errors and cycle slips were removed prior to processing, and ambiguities were resolved for each baseline using a quasi-ionosphere-free strategy. Troposphere parameters for each site were estimated every two hours. Surface velocities were calculated from the weighted combination of daily free-network coordinate solutions. The free solution was computed by minimizing the coordinate transformation of the IGS00 station coordinates, a precise subset of the ITRF2000 network, onto their known coordinates. The resulting solution includes coordinate and velocity estimates for all the stations and is consistent with the ITRF2000 reference frame. The resulting a posteriori sigma of unit weight for the combination was 0.0015.

The effects of angular rotation<sup>3,4</sup> between India and Asia were suppressed by determining relative velocities within the study area; between BIRP and points in eastern Nepal, and between BHAI and points in central Nepal, assuming the arc-normal velocities of BIRP and BHAI are identical. Resulting angular errors are <1° over the

scale of the network. Velocities from points in southern Tibet were included to constrain velocities immediately north of Nepal, and the data were resolved into their arc-normal component, N5°E and N18°E for eastern and central Nepal respectively. The relative velocity of BIRP/BHAI was then inferred from the synthetic velocity curve generated by the planar elastic dislocation model that best fits the observations. Hence in Figure 2, the velocity of BIRP/BHAI relative to fixed India is ~1.7 mm/yr.

Standard deviations in ITRF2000 were propagated into the new local reference frame. For the east (and north) components of velocity, the  $1\sigma$  uncertainty in the local reference frame is given for each station by

$$\sigma_E = \sqrt{\sigma_e^2 + \sigma_{fix}^2} \quad (1)$$

where  $\sigma_e$  is the standard deviation of the velocity in ITRF2000 and  $\sigma_{fix}$  is the standard deviation of the fixed station velocity (BHAI or BIRP) in ITRF2000. The standard deviation of the arc-normal velocity is given by

$$\sigma_{horz} = \sqrt{\frac{\sigma_E^2 \sigma_N^2}{\sigma_N^2 \cos^2 \theta + \sigma_E^2 \sin^2 \theta}} \quad (2)$$

where  $\sigma_E$  is the standard deviation of the east velocity,  $\sigma_N$  is the standard deviation of the north velocity, and  $\theta$  is the bearing of the convergence vector, counterclockwise from east.

### GPS data north of the Himalaya

Starting some 50 km north of the Himalaya a strain rate of 17-18  $\mu\text{m}/\text{yr}$  is established<sup>5,6</sup> that extends throughout much of Tibet. In our study area (83-90°E, 26-33°N shown in Figure 1 of main article) we include a re-analysis of a subset of the Chen et al.(2004)<sup>7</sup> velocities and find a strain rate at N10E of  $17.9 \pm 1 \times 10^{-8}/\text{yr}$  (Figure 1). The recent compilation by Bettinelli et al.<sup>1</sup> includes results from Chen et al. in southern Tibet which they convert to an ITRF2000 frame of reference. In this article we also include the results of Zhang et al. and Chen et al. up to 600 km from the frontal thrusts suitably adjusted for frames of reference and projected onto a N10E section.

We combined the ITRF2000 data sets of this study and Zhang et al. into an India-fixed frame. Velocities from this study were calculated relative to BHAI in central Nepal and BIRP in eastern Nepal. The Zhang et al. velocities were calculated relative to the Zhang velocity for BHAI. Uncertainties were propagated from the absolute velocity uncertainties of each study, according to Equation 1 above.

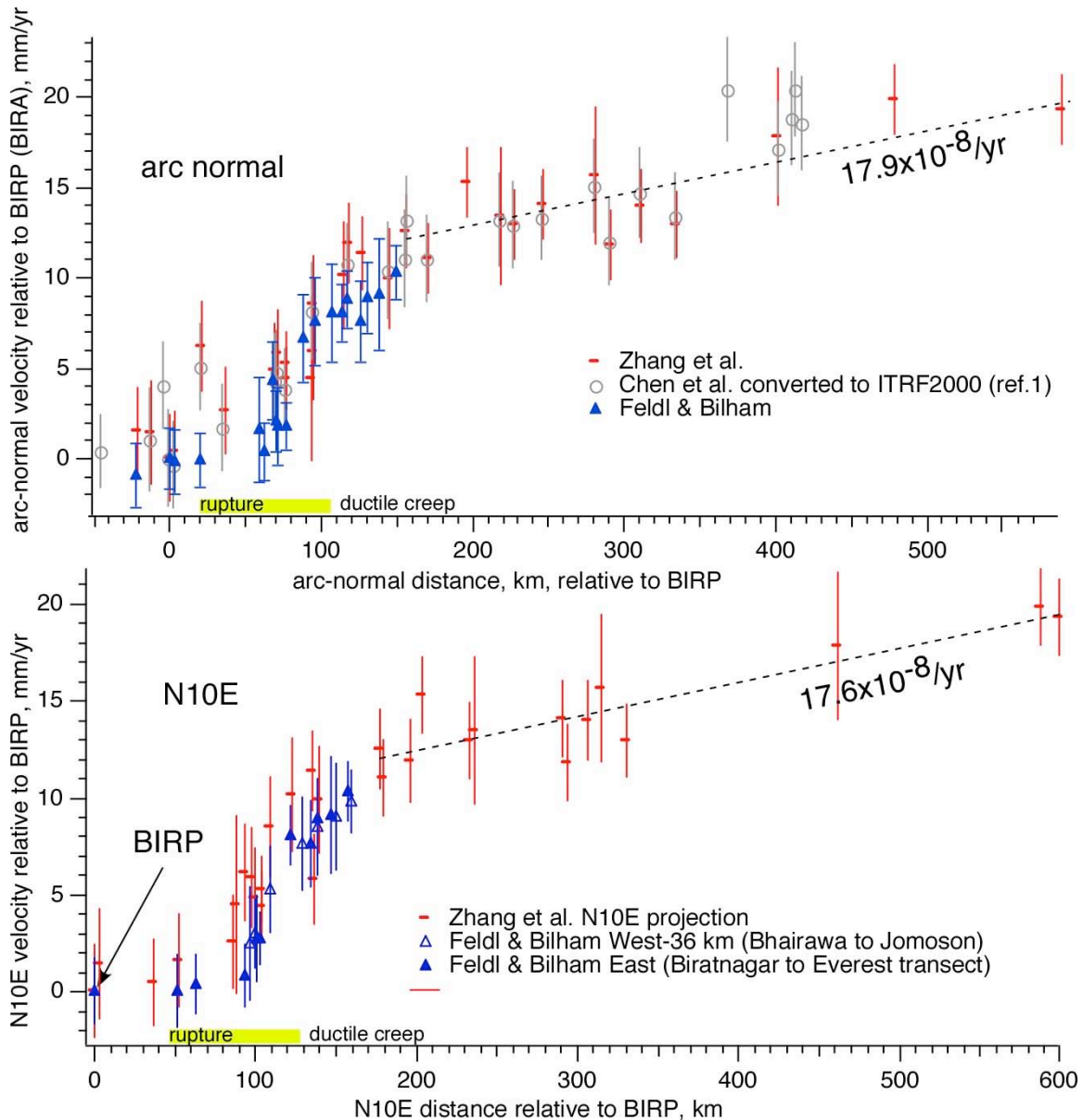


Figure 1 Arc-normal and N10E velocities relative to Biratnagar (BIRP/BIRA). The velocity of Biratnagar is approximately  $1 \pm 2$  mm/yr relative to the Indian Plate<sup>1</sup>. We use the ITRF 1997 points of Chen et al (2004)<sup>7</sup> converted to ITRF2000<sup>1</sup>. The frontal thrusts emerge at 20-30 km on the distance axis and the mean 3.5 km contour, the zero datum of all models in this article, crosses near Lukla at 120 km. The distance between these two points is the approximate width of rupture of Himalayan earthquakes (here in yellow; Bettinelli et al.<sup>1</sup> propose a width of 115 km). We have offset the western Nepal points by 36 km in the lower plot to adjust for the relative position of the locking line caused by the curvature of the arc.

## Planar Elastic Models

We initially modeled the southernmost 100 km of the observed Himalayan velocity field, as have previous investigators<sup>8</sup>, as the product of uniform slip on one or more planar faults embedded in an elastic half-space. For this planar elastic dislocation model, we

used the Nepal velocities calculated in this study and the velocities of RONG and TING (See figure 1 of published article) from Tibet<sup>5</sup>. A 2-D single fault approximation<sup>9</sup> provides an adequate fit to the somewhat scattered data as long as arc curvature is negligible over the length of the model, although a physically more satisfying fit can be obtained by incorporating additional structural and geometrical data and solving for vertical deformation simultaneously<sup>1</sup>. In eastern Nepal (86.5°-88.5°E) we adopted a strike of N95°E and in central Nepal (82.5°-86.5°) N108°E, parallel to trends of mapped microseismicity<sup>12,13</sup>. Although separate elastic models for central and eastern Nepal provide a marginally better fit to the observations than the ensemble analysis, the locking line for the entire data set better approximates the locus of the microseismicity peak with which it has been associated<sup>10,12</sup> (Table 2). We conclude from Figures 2 & 3 that the best fitting planar dislocation has a uniform velocity of  $17\pm 1$  mm/yr dipping 9° arc normal.

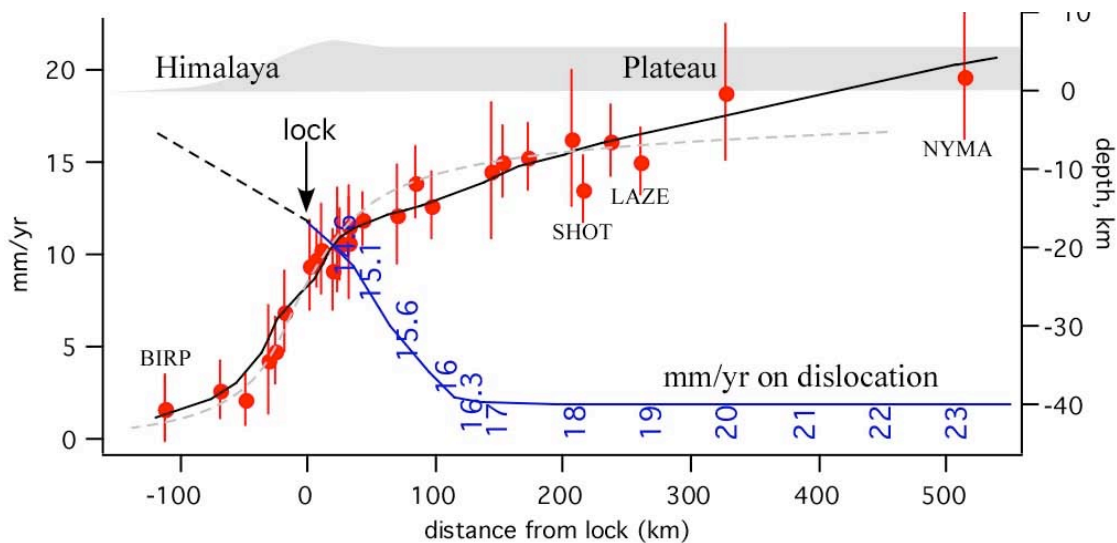


Figure 2. Combined GPS data (one standard deviation) from this study and Zhang et al. and synthetic fits for 17 mm/yr uniform slip on a 6° planar dislocation (dashed line), and for imposed northward increasing slip on a geometric surface beneath southern Tibet defined by receiver function analysis<sup>18</sup>. The surface velocity field (top right and cross-section below) is emulated by a series of contiguous dislocations increasing in slip velocity northwards at 17  $\mu\text{m}/\text{km}/\text{yr}$ , starting from a tip velocity near the locking line of  $13.5\pm 3$  mm/yr (one sigma). The applied displacement on the geometrical surface shown here is thus a forward model inferred and modified from the observed surface velocity field (Figure 1), rather than calculated from an elastic model as we do later (see Figure 2 of published article). We show it in this figure merely to demonstrate that it leads to a quite reasonable fit to the data.

We qualify this statement by pointing out that the small uncertainty and the derived rate applies only to the subset of points that we selected for our analysis. Had additional data been incorporated northward into Tibet, the best fitting velocity and its uncertainty would increase. This results from the incorporation of points that define the NNE strain contraction of Tibet. The Himalayan collision does not occur between two rigid plates<sup>10</sup>. The difficulty in deciding where to cut off the data in the north is avoided in later elastic models that emulate Tibet's NNE directed contraction and thereby fit these northern points. The most important finding from these models is the recognition that the selection of increasingly more northerly GPS points in the planar model raises the

inferred slip velocity, a reason why we should not expect many of the reported velocities in the past several years to have converged on a single precise "collision velocity" <sup>1,11-16</sup> despite the accumulation of data that should reduce velocity uncertainties with time.

It is well known that the singularity associated with the termination of uniform slip on a planar dislocation is avoided on a real fault because slip tapers to zero over a finite distance near the tip of the fault. An analytical form of this tapered-slip is available in the form of an elliptical decay in slip towards the locked tip, however, vertical uplift is much reduced in such models, so much so that they have found no application in the Himalaya. We found, however, that this elliptically tapered slip when applied to the sigmoidally shaped interface of the descending Indian plate as quantified from a receiver-function analysis across the Himalaya<sup>18</sup> yields a substantially better fit to both vertical and horizontal data. In Figure 2 we show both the planar fit and the fit from a forward model derived by trial and error. The starting point for deriving slip imposed on each planar segment in the curved interface model was derived from the observed surface velocity field. The curved interface model was fit to data combined from this study and from Zhang et al., (2004)<sup>6</sup> as compared to the planar dislocation model, which was fit to the smaller subset of data from this study and the velocities of RONG and TING<sup>5</sup> (for locations see Figure 1 of main published article and for discussion see Chen et al., 2004<sup>7</sup>).

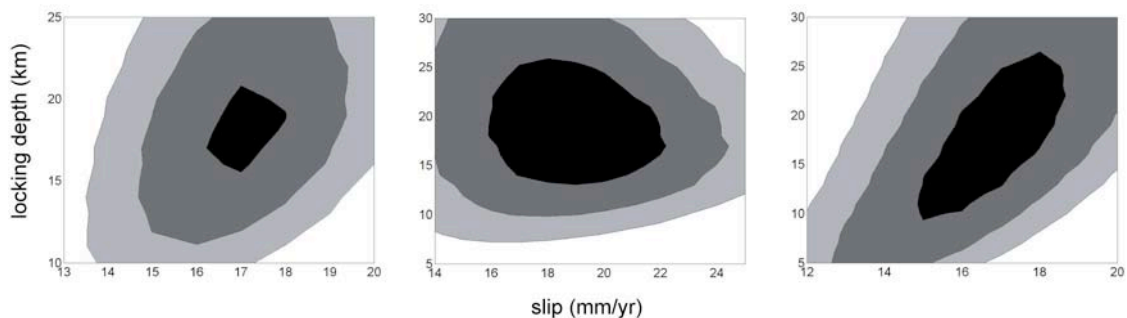


Figure 3 Trade-off between locking depth and slip parameters in planar dislocation modeling (Figure 2), for the combined data, central, and eastern Nepal (left to right). The contours mark the 1s, 2s, and 3s confidence limits. The best fitting dislocation for the combined data yields a slip of  $17\pm 1$  mm/yr with a locking depth of 18 km.

Tapered slip can also be emulated from a consideration of the frictional properties of the sub-Himalayan interface and its surrounding rheology<sup>10,19-21</sup>. However, the effects of friction are important only if the viscous component of slip on the interface has a long time constant compared to the interseismic duration of the earthquake cycle. During the period of post-seismic adjustment the rheology of the interface moderates slip rates, but if the time constant of viscous drag is less than a decade the interface behaves as though it were frictionless during the interseismic period. With this caveat, we conclude that the geometry of the interface is more important than its rheology. We calculate minimum-coseismic and maximum post-seismic slip in models.

We subsequently abandoned modeling estimates of surface velocity fields produced by complex subsurface geometries where a pre-conceived distribution of slip is applied to

subsurface elements, in favor of models in which this slip distribution is calculated from the geometry and stresses of the collision. This approach, which forms the main thrust of our article, emulates the collision zone as a series of boundary elements driven from the north.

### Boundary element models

We use the subsurface geometry of the Himalaya <sup>17</sup> as a starting point and defined a series of segment boundaries to drive and respond to plateau convergence (Figure 4 &5). We initially ran a series of models that started 1000 km north of the Himalaya and treated the Himalaya at depth as a 3600-long "cylindrical" extruded sigmoidal interface to avoid edge effects. We divided this surface into a sufficient number of segments so as to be able to drive the shortest earthquake rupture of interest - 50 km along strike (Figure 5). We found the models not particular sensitive to the segment density and although we were able to emulate GPS convergence rates throughtout Tibet, to economize on computing time we used a coarser grid for most of the models presented. Thus our initial models used >1800 elements (requiring 4 hour computing runs and much increased allocations for array space in 3d-def) and later ones fewer than 750. We found that the model results were also not particularly sensitive to the distance north of the northern boundary driving element so we eventually, and with encouragement from reviewer Jeff Freymueller, opted to drive the system from 594 km north of the Indian plate ( $\approx 500$  km north of the Himalaya). This shorter boundary condition avoids the adoption and interpolation of GPS data from further north into Tibet which is unavailable directly north of our region of interest. It also corresponds approximately with the Jiali seismic zone, a prominent tectonic boundary in central Tibet.

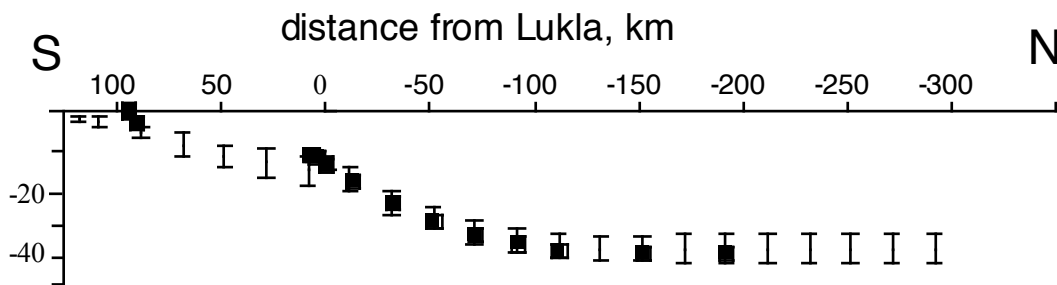


Figure 4 Subsurface geometry of the India/Tibetan plateau interface beneath the Himalaya and southern Tibet. The error bars show the range of depths estimated from [17] and the square markers indicate the preferred geometry required to obtain the best fitting models indicated in Fig 2 of the main article. We found the creeping interface to approach 15 km of the surface and to extend 7.5 km south of the locking line of best fitting planar models.

Having modified the subsurface geometry to one that best emulates the observed surface velocity field (Figure 5a) we record the resulting elemental slip velocity. From these velocities we calculate the displacements on these sub-surface segments corresponding to 1000 years of present-day slip, and for a second boundary-element model (Figure 5b) in which the area of freely slipping boundary elements is extended southwards, as occurs rapidly during an earthquake. We choose a 6-12° NNE dipping planar surface for this

extended rupture, with or without a ramp dipping more steeply to the surface near the Main Boundary faults of the Himalaya. The extended slip zone changes the location of the southernmost locked line in the case of short (<80 km) blind reverse fault, and makes it emerge at the surface in the case of a long (>90km) rupture.

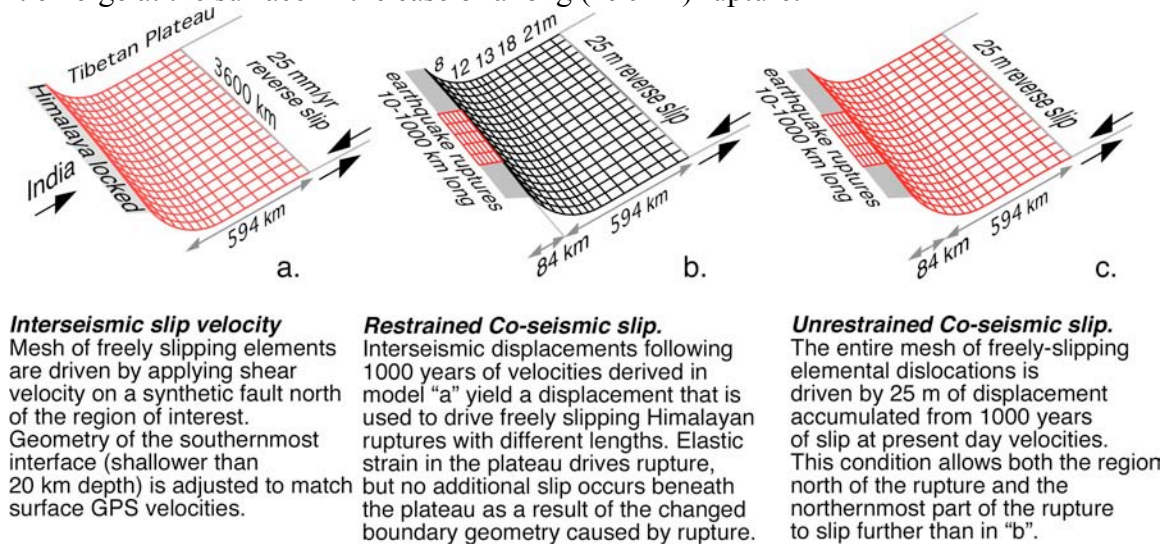


Figure 5. The mesh and conditions for the three boundary element models used. All are driven by a horizontal thrust fault 2000 km wide starting 594 km north of India, and an imposed contraction rate of  $4.9 \times 10^{-8}$  strain/year. Red elements slip freely. Black elements have specified slip. **a.** Interseismic surface velocities are emulated by adjusting the geometry of the southernmost elements as shown in Figure 4. **b.** Shows the restrained slip condition appropriate for instantaneous pre-seismic displacements driving a frictionless dislocation beneath the Himalaya. **c.** Slip of the rupture changes the southernmost boundary condition for the entire model. This unrestrained condition represents the fully relaxed afterslip condition.

The interseismic slip distribution throughout the plateau (calculated above) is modified by this extended rupture zone and responds by increasing displacements especially close to the former locked tip of the ductile creeping zone (Figure 5c). Not all of this displacement will be expressed at the time of the earthquake since it occurs in the zone of ductile creep. Thus much of the resulting redistribution of slip on the interface caused by very long ruptures is presumably manifest in afterslip<sup>21</sup>. The instantaneous (5b) and afterslip (5c) synthetic slip calculated for Himalayan ruptures in this way offer minimum and maximum estimates for moment magnitude respectively. It is probable that moment release immediately north of long ruptures will be partly seismic, permitting coseismic magnitudes somewhere between the two extremes to occur on the basal thrust fault beneath the Himalaya. The synthetic slip distribution on restrained planar rupture zones shows maximum slip near their northern edges. The dynamics of slip near the free surface, however, will permit these large coseismic slips ( $\geq 20$  m) to be manifest locally on the MBT as surface rupture.

### Elastic and inelastic strain and east-west extension

The fraction of the total strain released by earthquakes varies with the length of the rupture. We note in our models, however, that even for the largest earthquakes as much

as 80% of the strain north of the Himalaya remains untapped by coseismic slip (Figures 6 and 7). This residual strain remains to drive inelastic N/S convergence and east-west extension of Tibet. Although it is possible to quantify the proportion of inelastic and elastic strain in the earthquake cycle for single events, and is in fact dominated by the largest earthquakes, the actual apportionment in practice depends on the cumulative effects of many earthquake cycles involving a range of different length ruptures, and is beyond the scope of the present article.

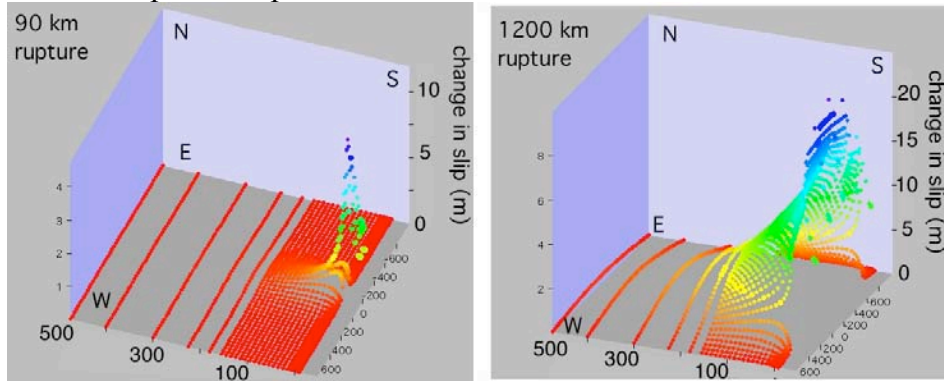


Figure 6. An example of boundary element changes in displacement for 90-km-long and 1200-km-long ruptures for unrestrained slip beneath the Tibetan Plateau extending south into each rupture. Each colored dot is a freely slipping element. We show the change of slip on all elements accompanying an earthquake that extends the southern locking line southward, as occurs in an earthquake. Where the rupture is short, earthquake slip is low, and displacements beneath Tibet are relatively modest. Where the rupture is long, rupture slip approaches the full applied preseismic displacement, and occurs over a wide region beneath Tibet although not all of it can be released coseismically. East-west and north-south distances are in km, whereas the z axis is in m, color coded to emphasize slip.

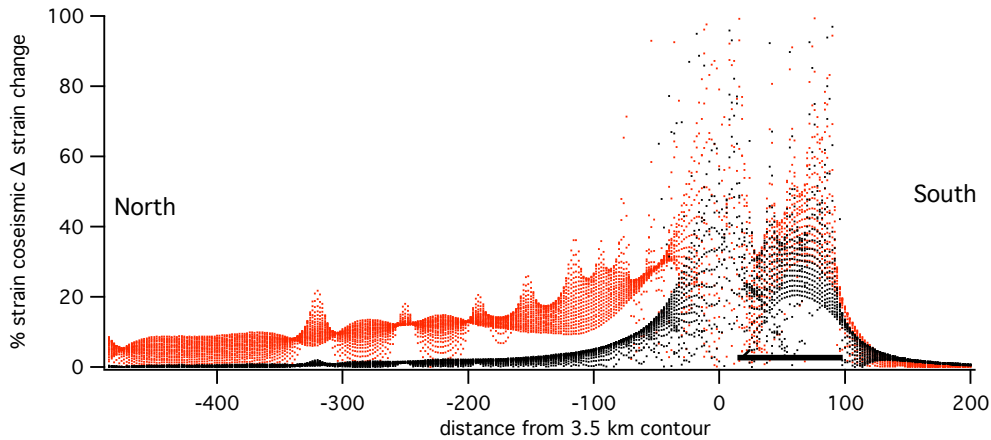


Figure 7 Percentage dilatational strain change throughout the uppermost 40 km of the plateau accompanying 100-km-long (black) and 600-km-long (red) ruptures. Even for a 600-km-long rupture, cyclic strain changes in the plateau are less than 20%, leaving the remaining 80% to drive anelastic deformation in the plateau. The cusps are artifacts of segment boundaries and their effects are much attenuated in models with smaller segments. The upper edge of each envelope in each case is the region north of each rupture, and the lower edge of the envelope are regions far E & NE and W & NW of each rupture. Synthetic earthquake ruptures propagate from -7.5 km to 94 km south of the 3.5 km contour (black bar right).

In Figure 5 in the main article we provide cross-sections and map views of the strain changes associated with 100 km and 600 km long ruptures to illustrate the strain changes that accompany earthquakes with different rupture lengths. Note that strain is depleted more for the case of the 600 km long rupture, and that this is evident more clearly in the section than in the map view, which shows only surface strain.

In these models the maximum cyclic *east-west* strains and displacements occur in the range 50-100 km north of the Himalaya. These result from Poissons' ratio effects that grow during the interseismic period and are released by great earthquakes in the Himalaya. We note they occur along that part of the southern plateau most densely populated by tensile grabens and half grabens. Given this association it would not be unexpected if seismicity in the grabens were linked to strain accumulation and release associated with great earthquakes in the Himalaya.

**Table 1** GPS station coordinates and ITRF2000 velocities from this study for east and north components with  $1\sigma$  uncertainty. The number of observing sessions are indicated in the ten columns right. Data from 1992 were collected in 8-hour sessions; 24-hour sessions were conducted in 1995-2004.

<i>Station</i>	<i>Lat. °N</i>	<i>Long. °E</i>	<i>East mm/yr</i>	<i>N. mm/yr</i>	92	95	96	97	98	99	00	01	03	04
JOMS	28.780	83.717	33.82±1.08	24.31±0.98	3	9			4				4	
P109	28.199	83.981	33.11±1.27	31.33±1.23					12				9	
BENI	28.347	83.561	35.93±1.86	28.57±1.80					9				5	
GANS	28.599	83.642	35.78±2.24	25.25±2.12					4				5	
JALT	28.507	83.658	34.98±2.17	26.34±2.06					5				6	
KUSU	28.210	83.677	35.25±2.53	31.45±2.61					2				4	
TUKO	28.709	83.644	33.65±2.38	25.13±2.46					4				4	
KPFB	27.993	86.827	37.48±0.94	22.21±0.95			10	4	3	3			27	1
LUKL	27.686	86.726	38.55±1.18	24.25±1.04		4	1				4		5	3
NAMC	27.802	86.715	39.61±2.46	24.58±1.86			20	13			6			
PHER	27.894	86.822	40.08±2.99	22.98±2.82			2	4			4		4	5
TANG	27.835	86.764	38.29±1.64	23.47±1.57			5				7		2	3
BHAI	27.507	83.417	37.85±1.67	33.52±1.34	3									3
TANS	27.873	83.553	35.02±0.99	33.18±0.93	3									3
BIRP	26.483	87.267	37.90±1.30	32.57±1.20			10	9	19	26				3
HILE	27.049	87.326	36.57±1.06	32.40±0.97		5						5		2
NAGA	27.692	85.521	36.06±0.43	31.09±0.39	9	11	33	14	13	11	12	10	12	
SIMA	27.162	84.981	41.49±1.46	32.11±1.27	3	4	11	17	16	17	5			
AIRP	27.697	85.357	30.72±1.82	32.04±1.78		3			5					

**Table 2** Reported Himalayan slip rates based on planar dislocation estimates for this study<sup>25</sup>.

Interval	Slip rate (mm/yr)	Locking depth (km)	Dip (°)	Location	$c^2$
1992-2004	17±2	18	9	eastern Nepal	1.053
	19±3	18	6	central Nepal	0.276
	17±1	18	9	combined	1.633

## **Input files section400 and 300map, and executable program.**

Typical 3d-def input text files<sup>22-24</sup> used in this study are provided as downloadable ascii files. *Section400* and *300map* calculate unrestrained slip on 400-km-long and 300-km-long ruptures respectively. They can be used directly as input to 3d-def .

The input file *300map* is for a 300-km-long unrestrained rupture with a total of 29 planes each divided into 50 segments along strike, driven by a reverse fault 1000 km north of the Himalaya. The first two planes are a rupture fronting the Himalaya divided into five segments along-strike and five elements down-dip, the first being a steep ramp and the second a gently dipping decollement. It outputs a map view of the surface strain (suffix .m300) and a segment displacement listing in a north-south line through the center of the rupture. Columns 2 and 3 after the line that starts "for each plane" indicate the start points (distance and depth) of each segment, and columns 5 and 9 indicate the length and dip respectively. The along-strike length of the interseismic driving condition is 3600 km and in this model each segment width is 56.25 km. All elements are freely-slipping (code 12) except the most northerly plane and last listed plane segment 30 (code 10) which drives the system at 35 mm/year, or in the case of coseismic rupture with an imposed displacement of 35 m. The first two planes specified are the Himalayan rupture, the first plane representing a 45° north-dipping 5.7-km-long ramp-thrust that cuts the surface . If these planes are removed and the number of planes reduced from 17 to 15 in line 2, the file can be used to calculate pre-seismic displacements or interseismic velocities. Strain and displacement changes accompanying rupture can then be obtained by subtracting the two output matrices. This file executes in about 4 hours on a 1 GHz Apple Powerbook-Pro running in UNIX. For experimental purposes to speed up the computation, the size of each section or map can be decimated by dividing the numbers in the last line of code by ten.

The second file, *section400*, differs in its length (1700 km), width (it is driven from 500 km north of the Himalaya, and the output section with suffix .i400 it calculates instead of map view. It also has fewer segments to speed computation. Sixty four along-strike segments are placed beneath the southern plateau, reducing to thirty-two 72 km north of the locking line. As before the rupture consists of two planes each with 25 segments. The system here is driven at 25 mm/year. Both files output shear and dilatational strain, displacement or velocity, and displacement of velocity on the subsurface segments.

### ***3ddef.tar***

The 3ddef Fortran code downloaded from the CERI web site<sup>23</sup> must be modified to process the large matrices inverted in the present analysis. The *code provided* (256kb) has been modified appropriately and can invert the large arrays used to examine slip on hundreds of freely-slipping elements in this article. We are indebted to Walter Szeliga, University of Colorado, for these modifications. A compiled Fortran 91 version of this code that runs in the UNIX terminal mode of Apple computers can be downloaded as a .tar file. Place the input files *section400* or *300map* in the folder 3ddef once it has been

de-compressed. To run the program 3ddef on the desktop screen from "Terminal", change to the directory to 3ddef [cd desktop/3ddef] then type ./3d and enter the appropriately named input file when prompted. The program will run in the background, but will be faster if no other tasks are running.

—

## References

1. Bettinelli, P., J.P. Avouac, M. Flouzat, F. Jouanne, L. Bollinger, P. Willis, and G.R. Chitraker, Plate motion of India and interseismic strain in the Nepal Himalaya from GPS and DORIS measurements, *Journal of Geodesy*, doi: 10.1007/s00190-006-0030-3, 2006.
2. Beutler, G. et al. (eds. Hugentobler, U., Schaer, S. & Fridez, P.) (Astronomical Institute, University of Berne, Switzerland, 2001).
3. Gordon, R. G., Argus, D. F. & Heflin, M. B. Revised estimate of the angular velocity of India relative to Eurasia. *EOS, Transactions of the American Geophysical Union* **80**, F273 (1999).
4. Sella, G. F., Dixon, T. H. & Mao, A. REVEL: A model for Recent plate velocities from space geodesy. *Journal of Geophysical Research* **107** (2002).
5. Wang, Q. et al. Present-Day Crustal Deformation in China Constrained by Global Positioning System Measurements. *Science* **294**, 574-577 (2001).
6. Zhang, Pei-Zhen, Shen, Zhengkang, Wang, Min, Gan, Weijun, Bürgmann, R., Molnar, P, Wang, Qi, Niu, Zhijun, Sun, Jianzhong, Wu, Jianchun, Hanrong, Sun, Xinzhao, You, Continuous deformation of the Tibetan Plateau from global positioning system data, *Geology* 2004 32: 809-812
7. Chen, Q., J. T. Freymueller, Z. Yang, C. Xu, W. Jiang, Q. Wang, and J. Liu (2004), Spatially variable extension in southern Tibet based on GPS measurements, *J. Geophys. Res.*, 109, B09401, doi:10.1029/2002JB002350.
8. Vergne J., R. Cattin and J.P. Avouac, On the use of dislocations to model interseismic strain and stress build-up at intracontinental thrust faults, *Geophys. J. Int.*, 147, 155-162, 2001.
9. Savage, J. C. A dislocation model of strain accumulation and release at a subduction zone. *Journal of Geophysical Research* **88**, 4984-4996 (1983).
10. Avouac, J. P. Mountain Building, Erosion, and the Seismic Cycle in the Nepal Himalaya. *Advances in Geophysics* **46**, 1-80 (2003).
11. Jouanne, F. et al. Current shortening across the Himalayas of Nepal. *Geophysical Journal International* **157**, 1-14 (2004).
12. Pandey, M. R., Tandukar, R. P., Avouac, J. P., Vergne, J. & Heritier, T. Seismotectonics of the Nepal Himalaya from a local seismic network. *Journal of Asian Earth Sciences* **17**, 703-712 (1999).
13. Bilham, R., Larson, K., Freymueller, J. & Project Idylhim members. GPS measurements of present-day convergence across the Nepal Himalaya. *Nature* **386**, 61-64 (1997).
14. Burgmann, R., Larson, K. & Bilham, R. Model Inversion of GPS and Leveling Measurements Across the Himalaya: Implications for Earthquake Hazards and Future Geodetic Networks. *Himalayan Geology* **20**, 59-72 (1999).

15. Larson, K., Burgmann, R., Bilham, R. & Freymueller, J. Kinematics of the India-Eurasia collision zone from GPS measurements. *Journal of Geophysical Research* **104**, 1077-1093 (1999).
16. Jade, S. et al. GPS measurements from the Ladakh Himalaya, India: Preliminary tests of plate-like or continuous deformation in Tibet. *Geological Society of America Bulletin* **116**, 1385-1391 (2004).
17. Banerjee, P. & Burgmann, R. Convergence across the northwest Himalaya from GPS measurements. *Geophysical Research Letters* **29** (2002).
18. Schulte-Pelkum, V. et al. Imaging the Indian Subcontinent beneath the Himalaya. *Nature* (2005).
19. Cattin, R. & Avouac, J. P. Modeling mountain building and the seismic cycle in the Himalaya of Nepal. *Journal of Geophysical Research* **105**, 13389-13407 (2000).
20. Perfettini, H. & Avouac, J. P. Postseismic relaxation driven by brittle creep: A possible mechanism to reconcile geodetic measurements and the decay rate of aftershocks, application to the Chi-Chi earthquake, Taiwan. *Journal of Geophysical Research* **109** (2004).
21. Perfettini, H. & Avouac, J. P. Stress transfer and strain rate variations during the seismic cycle. *Journal of Geophysical Research* **109** (2004).
22. Gomberg, J. & Ellis, M. Topography and tectonics of the central New Madrid seismic zone: Results of numerical experiments using a three-dimensional boundary-element program. *Journal of Geophysical Research* **99**, 20299-20310 (1994).
23. <http://www.ceri.memphis.edu/people/ellis/3ddef/gettingstuff.htm>
24. <http://www.ceri.memphis.edu/people/ellis/3ddef/index.html>
25. [http://cires.colorado.edu/~feldl/feldl\\_thesis.pdf](http://cires.colorado.edu/~feldl/feldl_thesis.pdf)









































1	1	12	0.	0.0	0.0	
1	1	12	0.	0.0	0.0	
1	1	12	0.	0.0	0.0	
1	1	12	0.	0.0	0.0	
1	1	12	0.	0.0	0.0	
1	1	12	0.	0.0	0.0	
1	1	12	0.	0.0	0.0	
1	1	12	0.	0.0	0.0	
1	1	12	0.	0.0	0.0	
1	1	12	0.	0.0	0.0	
30	1	1	10	0.	35	0.0

\* Run everything else interactively

Non-interactive grid specification

plane

XYZ

\* Coordinate system of output

global

\* Output files to create

displacements

elements

strain

\* Output file suffix

m300

\* Xo, Yo, Zo (Ref.corner), strike,dip,length,width:

-900 100 0 90 0 1800 600

\* number of grid points in the strike and dip directions (4km map grid)

450 150

```

* POISSONS RATIO      YOUNGS MOD      #PLANES      COEFF INTERNAL FRICTION      BACKGROUND DEFORMATION
.25                   7.E11        17           0.6                          strain
* Background (blank; Exx,Exy,Exz,Eyy,Eyz,Ezz; Sxx,Sxy,Sxz,Syy,Syz,Szz; dUx/dx /dy /dz,dUy/dx /dy
/dz,dUz/dx /dy /dz)
0 0 0 -4.9E-08 0 0 0 0 0

```

for each plane:

ORG:XO	YO	ZO	WDTH	LENGTH	#SUB-ELEM:STK	DIP	STK	DIP
-200	94	0.0	400.1	5.657	5 5 90	45		
-200	90	-4.0	400.1	83.23	5 5 90	7.595		
-1800	7.5	-15	3600.1	1.3	64 1 90	22.62		
-1800	6.3	-15.5	3600.1	2.508	64 1 90	23.499		
-1800	4	-16.5	3600.1	4.472	64 1 90	26.565		
-1800	0	-18.5	3600.1		14.318 64 1 90	24.775		
-1800	-13	-24.5	3600.1		20.427 64 1 90	21.541		
-1800	-32	-32	3600.1		20.881 64 1 90	16.699		
-1800	-52	-38	3600.1		20.616 64 1 90	14.036		
-1800	-72	-43	3600.1		20.224 32 1 90	8.531		
-1800	-92	-46	3600.1	20.1	32 1 90	5.711		
-1800	-112	-48	3600.1	40.012	32 1 90	1.432		
-1800	-152	-49	3600.1	40.00	32 1 90	0.		
-1800	-192	-49	3600.1	58	32 1 90	0.		
-1800	-250.0	-49	3600.1	70.0	32 1 90	0.		
-1800	-320.0	-49	3600.1	180	32 1 90	0.0		
-1800	-500.0	-49	3600.1	3000	1 1 90	0.0		

for each plane (at each fixed distance along strike, going up-dip):

PLN,SUB-ELEM code BC-shear(STK) BC2-shear(DIP) BC3-normal

1								
1	1	12	0.	0.0	0.0			
1	2	12	0.	0.0	0.0			
1	3	12	0.	0.0	0.0			
1	4	12	0.	0.0	0.0			
1	5	12	0.	0.0	0.0			
2	1	12	0.	0.0	0.0			
2	2	12	0.	0.0	0.0			
2	3	12	0.	0.0	0.0			
2	4	12	0.	0.0	0.0			
2	5	12	0.	0.0	0.0			
3	1	12	0.	0.0	0.0			
3	2	12	0.	0.0	0.0			
3	3	12	0.	0.0	0.0			
3	4	12	0.	0.0	0.0			
3	5	12	0.	0.0	0.0			
4	1	12	0.	0.0	0.0			
4	2	12	0.	0.0	0.0			
4	3	12	0.	0.0	0.0			
4	4	12	0.	0.0	0.0			
4	5	12	0.	0.0	0.0			
5	1	12	0.	0.0	0.0			
5	2	12	0.	0.0	0.0			
5	3	12	0.	0.0	0.0			
5	4	12	0.	0.0	0.0			
5	5	12	0.	0.0	0.0			
2								
1	1	12	0.	0.0	0.0			
1	2	12	0.	0.0	0.0			
1	3	12	0.	0.0	0.0			
1	4	12	0.	0.0	0.0			
1	5	12	0.	0.0	0.0			
2	1	12	0.	0.0	0.0			
2	2	12	0.	0.0	0.0			
2	3	12	0.	0.0	0.0			
2	4	12	0.	0.0	0.0			
2	5	12	0.	0.0	0.0			
3	1	12	0.	0.0	0.0			
3	2	12	0.	0.0	0.0			
3	3	12	0.	0.0	0.0			
3	4	12	0.	0.0	0.0			
3	5	12	0.	0.0	0.0			
4	1	12	0.	0.0	0.0			
4	2	12	0.	0.0	0.0			
4	3	12	0.	0.0	0.0			

4	4	12	0.	0.0	0.0
4	5	12	0.	0.0	0.0
5	1	12	0.	0.0	0.0
5	2	12	0.	0.0	0.0
5	3	12	0.	0.0	0.0
5	4	12	0.	0.0	0.0
5	5	12	0.	0.0	0.0

3

1	1	12	0.	0.0	0.0
1	2	12	0.	0.0	0.0
1	3	12	0.	0.0	0.0
1	4	12	0.	0.0	0.0
1	5	12	0.	0.0	0.0
1	6	12	0.	0.0	0.0
1	7	12	0.	0.0	0.0
1	8	12	0.	0.0	0.0
1	9	12	0.	0.0	0.0
1	10	12	0.	0.0	0.0
1	11	12	0.	0.0	0.0
1	12	12	0.	0.0	0.0
1	13	12	0.	0.0	0.0
1	14	12	0.	0.0	0.0
1	15	12	0.	0.0	0.0
1	16	12	0.	0.0	0.0
1	17	12	0.	0.0	0.0
1	18	12	0.	0.0	0.0
1	19	12	0.	0.0	0.0
1	20	12	0.	0.0	0.0
1	21	12	0.	0.0	0.0
1	22	12	0.	0.0	0.0
1	23	12	0.	0.0	0.0
1	24	12	0.	0.0	0.0
1	25	12	0.	0.0	0.0
1	26	12	0.	0.0	0.0
1	27	12	0.	0.0	0.0
1	28	12	0.	0.0	0.0
1	29	12	0.	0.0	0.0
1	30	12	0.	0.0	0.0
1	31	12	0.	0.0	0.0
1	32	12	0.	0.0	0.0
1	33	12	0.	0.0	0.0
1	34	12	0.	0.0	0.0
1	35	12	0.	0.0	0.0
1	36	12	0.	0.0	0.0
1	37	12	0.	0.0	0.0
1	38	12	0.	0.0	0.0
1	39	12	0.	0.0	0.0
1	40	12	0.	0.0	0.0
1	41	12	0.	0.0	0.0
1	42	12	0.	0.0	0.0
1	43	12	0.	0.0	0.0
1	44	12	0.	0.0	0.0
1	45	12	0.	0.0	0.0
1	46	12	0.	0.0	0.0
1	47	12	0.	0.0	0.0
1	48	12	0.	0.0	0.0
1	49	12	0.	0.0	0.0
1	50	12	0.	0.0	0.0
1	51	12	0.	0.0	0.0
1	52	12	0.	0.0	0.0
1	53	12	0.	0.0	0.0
1	54	12	0.	0.0	0.0
1	55	12	0.	0.0	0.0
1	56	12	0.	0.0	0.0
1	57	12	0.	0.0	0.0
1	58	12	0.	0.0	0.0
1	59	12	0.	0.0	0.0
1	60	12	0.	0.0	0.0
1	61	12	0.	0.0	0.0
1	62	12	0.	0.0	0.0
1	63	12	0.	0.0	0.0
1	64	12	0.	0.0	0.0

4

1	1	12	0.	0.0	0.0
1	2	12	0.	0.0	0.0
1	3	12	0.	0.0	0.0
1	4	12	0.	0.0	0.0
1	5	12	0.	0.0	0.0
1	6	12	0.	0.0	0.0
1	7	12	0.	0.0	0.0
1	8	12	0.	0.0	0.0
1	9	12	0.	0.0	0.0
1	10	12	0.	0.0	0.0
1	11	12	0.	0.0	0.0
1	12	12	0.	0.0	0.0
1	13	12	0.	0.0	0.0
1	14	12	0.	0.0	0.0
1	15	12	0.	0.0	0.0
1	16	12	0.	0.0	0.0
1	17	12	0.	0.0	0.0
1	18	12	0.	0.0	0.0
1	19	12	0.	0.0	0.0
1	20	12	0.	0.0	0.0
1	21	12	0.	0.0	0.0
1	22	12	0.	0.0	0.0
1	23	12	0.	0.0	0.0
1	24	12	0.	0.0	0.0
1	25	12	0.	0.0	0.0
1	26	12	0.	0.0	0.0
1	27	12	0.	0.0	0.0
1	28	12	0.	0.0	0.0
1	29	12	0.	0.0	0.0
1	30	12	0.	0.0	0.0
1	31	12	0.	0.0	0.0
1	32	12	0.	0.0	0.0
1	33	12	0.	0.0	0.0
1	34	12	0.	0.0	0.0
1	35	12	0.	0.0	0.0
1	36	12	0.	0.0	0.0
1	37	12	0.	0.0	0.0
1	38	12	0.	0.0	0.0
1	39	12	0.	0.0	0.0
1	40	12	0.	0.0	0.0
1	41	12	0.	0.0	0.0
1	42	12	0.	0.0	0.0
1	43	12	0.	0.0	0.0
1	44	12	0.	0.0	0.0
1	45	12	0.	0.0	0.0
1	46	12	0.	0.0	0.0
1	47	12	0.	0.0	0.0
1	48	12	0.	0.0	0.0
1	49	12	0.	0.0	0.0
1	50	12	0.	0.0	0.0
1	51	12	0.	0.0	0.0
1	52	12	0.	0.0	0.0
1	53	12	0.	0.0	0.0
1	54	12	0.	0.0	0.0
1	55	12	0.	0.0	0.0
1	56	12	0.	0.0	0.0
1	57	12	0.	0.0	0.0
1	58	12	0.	0.0	0.0
1	59	12	0.	0.0	0.0
1	60	12	0.	0.0	0.0
1	61	12	0.	0.0	0.0
1	62	12	0.	0.0	0.0
1	63	12	0.	0.0	0.0
1	64	12	0.	0.0	0.0

5

1	1	12	0.	0.0	0.0
1	2	12	0.	0.0	0.0
1	3	12	0.	0.0	0.0
1	4	12	0.	0.0	0.0
1	5	12	0.	0.0	0.0
1	6	12	0.	0.0	0.0
1	7	12	0.	0.0	0.0
1	8	12	0.	0.0	0.0

1	9	12	0.	0.0	0.0
1	10	12	0.	0.0	0.0
1	11	12	0.	0.0	0.0
1	12	12	0.	0.0	0.0
1	13	12	0.	0.0	0.0
1	14	12	0.	0.0	0.0
1	15	12	0.	0.0	0.0
1	16	12	0.	0.0	0.0
1	17	12	0.	0.0	0.0
1	18	12	0.	0.0	0.0
1	19	12	0.	0.0	0.0
1	20	12	0.	0.0	0.0
1	21	12	0.	0.0	0.0
1	22	12	0.	0.0	0.0
1	23	12	0.	0.0	0.0
1	24	12	0.	0.0	0.0
1	25	12	0.	0.0	0.0
1	26	12	0.	0.0	0.0
1	27	12	0.	0.0	0.0
1	28	12	0.	0.0	0.0
1	29	12	0.	0.0	0.0
1	30	12	0.	0.0	0.0
1	31	12	0.	0.0	0.0
1	32	12	0.	0.0	0.0
1	33	12	0.	0.0	0.0
1	34	12	0.	0.0	0.0
1	35	12	0.	0.0	0.0
1	36	12	0.	0.0	0.0
1	37	12	0.	0.0	0.0
1	38	12	0.	0.0	0.0
1	39	12	0.	0.0	0.0
1	40	12	0.	0.0	0.0
1	41	12	0.	0.0	0.0
1	42	12	0.	0.0	0.0
1	43	12	0.	0.0	0.0
1	44	12	0.	0.0	0.0
1	45	12	0.	0.0	0.0
1	46	12	0.	0.0	0.0
1	47	12	0.	0.0	0.0
1	48	12	0.	0.0	0.0
1	49	12	0.	0.0	0.0
1	50	12	0.	0.0	0.0
1	51	12	0.	0.0	0.0
1	52	12	0.	0.0	0.0
1	53	12	0.	0.0	0.0
1	54	12	0.	0.0	0.0
1	55	12	0.	0.0	0.0
1	56	12	0.	0.0	0.0
1	57	12	0.	0.0	0.0
1	58	12	0.	0.0	0.0
1	59	12	0.	0.0	0.0
1	60	12	0.	0.0	0.0
1	61	12	0.	0.0	0.0
1	62	12	0.	0.0	0.0
1	63	12	0.	0.0	0.0
1	64	12	0.	0.0	0.0

6

1	1	12	0.	0.0	0.0
1	2	12	0.	0.0	0.0
1	3	12	0.	0.0	0.0
1	4	12	0.	0.0	0.0
1	5	12	0.	0.0	0.0
1	6	12	0.	0.0	0.0
1	7	12	0.	0.0	0.0
1	8	12	0.	0.0	0.0
1	9	12	0.	0.0	0.0
1	10	12	0.	0.0	0.0
1	11	12	0.	0.0	0.0
1	12	12	0.	0.0	0.0
1	13	12	0.	0.0	0.0
1	14	12	0.	0.0	0.0
1	15	12	0.	0.0	0.0
1	16	12	0.	0.0	0.0

1	17	12	0.	0.0	0.0
1	18	12	0.	0.0	0.0
1	19	12	0.	0.0	0.0
1	20	12	0.	0.0	0.0
1	21	12	0.	0.0	0.0
1	22	12	0.	0.0	0.0
1	23	12	0.	0.0	0.0
1	24	12	0.	0.0	0.0
1	25	12	0.	0.0	0.0
1	26	12	0.	0.0	0.0
1	27	12	0.	0.0	0.0
1	28	12	0.	0.0	0.0
1	29	12	0.	0.0	0.0
1	30	12	0.	0.0	0.0
1	31	12	0.	0.0	0.0
1	32	12	0.	0.0	0.0
1	33	12	0.	0.0	0.0
1	34	12	0.	0.0	0.0
1	35	12	0.	0.0	0.0
1	36	12	0.	0.0	0.0
1	37	12	0.	0.0	0.0
1	38	12	0.	0.0	0.0
1	39	12	0.	0.0	0.0
1	40	12	0.	0.0	0.0
1	41	12	0.	0.0	0.0
1	42	12	0.	0.0	0.0
1	43	12	0.	0.0	0.0
1	44	12	0.	0.0	0.0
1	45	12	0.	0.0	0.0
1	46	12	0.	0.0	0.0
1	47	12	0.	0.0	0.0
1	48	12	0.	0.0	0.0
1	49	12	0.	0.0	0.0
1	50	12	0.	0.0	0.0
1	51	12	0.	0.0	0.0
1	52	12	0.	0.0	0.0
1	53	12	0.	0.0	0.0
1	54	12	0.	0.0	0.0
1	55	12	0.	0.0	0.0
1	56	12	0.	0.0	0.0
1	57	12	0.	0.0	0.0
1	58	12	0.	0.0	0.0
1	59	12	0.	0.0	0.0
1	60	12	0.	0.0	0.0
1	61	12	0.	0.0	0.0
1	62	12	0.	0.0	0.0
1	63	12	0.	0.0	0.0
1	64	12	0.	0.0	0.0

7

1	1	12	0.	0.0	0.0
1	2	12	0.	0.0	0.0
1	3	12	0.	0.0	0.0
1	4	12	0.	0.0	0.0
1	5	12	0.	0.0	0.0
1	6	12	0.	0.0	0.0
1	7	12	0.	0.0	0.0
1	8	12	0.	0.0	0.0
1	9	12	0.	0.0	0.0
1	10	12	0.	0.0	0.0
1	11	12	0.	0.0	0.0
1	12	12	0.	0.0	0.0
1	13	12	0.	0.0	0.0
1	14	12	0.	0.0	0.0
1	15	12	0.	0.0	0.0
1	16	12	0.	0.0	0.0
1	17	12	0.	0.0	0.0
1	18	12	0.	0.0	0.0
1	19	12	0.	0.0	0.0
1	20	12	0.	0.0	0.0
1	21	12	0.	0.0	0.0
1	22	12	0.	0.0	0.0
1	23	12	0.	0.0	0.0
1	24	12	0.	0.0	0.0

1	25	12	0.	0.0	0.0
1	26	12	0.	0.0	0.0
1	27	12	0.	0.0	0.0
1	28	12	0.	0.0	0.0
1	29	12	0.	0.0	0.0
1	30	12	0.	0.0	0.0
1	31	12	0.	0.0	0.0
1	32	12	0.	0.0	0.0
1	33	12	0.	0.0	0.0
1	34	12	0.	0.0	0.0
1	35	12	0.	0.0	0.0
1	36	12	0.	0.0	0.0
1	37	12	0.	0.0	0.0
1	38	12	0.	0.0	0.0
1	39	12	0.	0.0	0.0
1	40	12	0.	0.0	0.0
1	41	12	0.	0.0	0.0
1	42	12	0.	0.0	0.0
1	43	12	0.	0.0	0.0
1	44	12	0.	0.0	0.0
1	45	12	0.	0.0	0.0
1	46	12	0.	0.0	0.0
1	47	12	0.	0.0	0.0
1	48	12	0.	0.0	0.0
1	49	12	0.	0.0	0.0
1	50	12	0.	0.0	0.0
1	51	12	0.	0.0	0.0
1	52	12	0.	0.0	0.0
1	53	12	0.	0.0	0.0
1	54	12	0.	0.0	0.0
1	55	12	0.	0.0	0.0
1	56	12	0.	0.0	0.0
1	57	12	0.	0.0	0.0
1	58	12	0.	0.0	0.0
1	59	12	0.	0.0	0.0
1	60	12	0.	0.0	0.0
1	61	12	0.	0.0	0.0
1	62	12	0.	0.0	0.0
1	63	12	0.	0.0	0.0
1	64	12	0.	0.0	0.0

8

1	1	12	0.	0.0	0.0
1	2	12	0.	0.0	0.0
1	3	12	0.	0.0	0.0
1	4	12	0.	0.0	0.0
1	5	12	0.	0.0	0.0
1	6	12	0.	0.0	0.0
1	7	12	0.	0.0	0.0
1	8	12	0.	0.0	0.0
1	9	12	0.	0.0	0.0
1	10	12	0.	0.0	0.0
1	11	12	0.	0.0	0.0
1	12	12	0.	0.0	0.0
1	13	12	0.	0.0	0.0
1	14	12	0.	0.0	0.0
1	15	12	0.	0.0	0.0
1	16	12	0.	0.0	0.0
1	17	12	0.	0.0	0.0
1	18	12	0.	0.0	0.0
1	19	12	0.	0.0	0.0
1	20	12	0.	0.0	0.0
1	21	12	0.	0.0	0.0
1	22	12	0.	0.0	0.0
1	23	12	0.	0.0	0.0
1	24	12	0.	0.0	0.0
1	25	12	0.	0.0	0.0
1	26	12	0.	0.0	0.0
1	27	12	0.	0.0	0.0
1	28	12	0.	0.0	0.0
1	29	12	0.	0.0	0.0
1	30	12	0.	0.0	0.0
1	31	12	0.	0.0	0.0
1	32	12	0.	0.0	0.0

1	33	12	0.	0.0	0.0
1	34	12	0.	0.0	0.0
1	35	12	0.	0.0	0.0
1	36	12	0.	0.0	0.0
1	37	12	0.	0.0	0.0
1	38	12	0.	0.0	0.0
1	39	12	0.	0.0	0.0
1	40	12	0.	0.0	0.0
1	41	12	0.	0.0	0.0
1	42	12	0.	0.0	0.0
1	43	12	0.	0.0	0.0
1	44	12	0.	0.0	0.0
1	45	12	0.	0.0	0.0
1	46	12	0.	0.0	0.0
1	47	12	0.	0.0	0.0
1	48	12	0.	0.0	0.0
1	49	12	0.	0.0	0.0
1	50	12	0.	0.0	0.0
1	51	12	0.	0.0	0.0
1	52	12	0.	0.0	0.0
1	53	12	0.	0.0	0.0
1	54	12	0.	0.0	0.0
1	55	12	0.	0.0	0.0
1	56	12	0.	0.0	0.0
1	57	12	0.	0.0	0.0
1	58	12	0.	0.0	0.0
1	59	12	0.	0.0	0.0
1	60	12	0.	0.0	0.0
1	61	12	0.	0.0	0.0
1	62	12	0.	0.0	0.0
1	63	12	0.	0.0	0.0
1	64	12	0.	0.0	0.0

9

1	1	12	0.	0.0	0.0
1	2	12	0.	0.0	0.0
1	3	12	0.	0.0	0.0
1	4	12	0.	0.0	0.0
1	5	12	0.	0.0	0.0
1	6	12	0.	0.0	0.0
1	7	12	0.	0.0	0.0
1	8	12	0.	0.0	0.0
1	9	12	0.	0.0	0.0
1	10	12	0.	0.0	0.0
1	11	12	0.	0.0	0.0
1	12	12	0.	0.0	0.0
1	13	12	0.	0.0	0.0
1	14	12	0.	0.0	0.0
1	15	12	0.	0.0	0.0
1	16	12	0.	0.0	0.0
1	17	12	0.	0.0	0.0
1	18	12	0.	0.0	0.0
1	19	12	0.	0.0	0.0
1	20	12	0.	0.0	0.0
1	21	12	0.	0.0	0.0
1	22	12	0.	0.0	0.0
1	23	12	0.	0.0	0.0
1	24	12	0.	0.0	0.0
1	25	12	0.	0.0	0.0
1	26	12	0.	0.0	0.0
1	27	12	0.	0.0	0.0
1	28	12	0.	0.0	0.0
1	29	12	0.	0.0	0.0
1	30	12	0.	0.0	0.0
1	31	12	0.	0.0	0.0
1	32	12	0.	0.0	0.0
1	33	12	0.	0.0	0.0
1	34	12	0.	0.0	0.0
1	35	12	0.	0.0	0.0
1	36	12	0.	0.0	0.0
1	37	12	0.	0.0	0.0
1	38	12	0.	0.0	0.0
1	39	12	0.	0.0	0.0
1	40	12	0.	0.0	0.0

1	41	12	0.	0.0	0.0
1	42	12	0.	0.0	0.0
1	43	12	0.	0.0	0.0
1	44	12	0.	0.0	0.0
1	45	12	0.	0.0	0.0
1	46	12	0.	0.0	0.0
1	47	12	0.	0.0	0.0
1	48	12	0.	0.0	0.0
1	49	12	0.	0.0	0.0
1	50	12	0.	0.0	0.0
1	51	12	0.	0.0	0.0
1	52	12	0.	0.0	0.0
1	53	12	0.	0.0	0.0
1	54	12	0.	0.0	0.0
1	55	12	0.	0.0	0.0
1	56	12	0.	0.0	0.0
1	57	12	0.	0.0	0.0
1	58	12	0.	0.0	0.0
1	59	12	0.	0.0	0.0
1	60	12	0.	0.0	0.0
1	61	12	0.	0.0	0.0
1	62	12	0.	0.0	0.0
1	63	12	0.	0.0	0.0
1	64	12	0.	0.0	0.0

10

1	1	12	0.	0.0	0.0
1	2	12	0.	0.0	0.0
1	3	12	0.	0.0	0.0
1	4	12	0.	0.0	0.0
1	5	12	0.	0.0	0.0
1	6	12	0.	0.0	0.0
1	7	12	0.	0.0	0.0
1	8	12	0.	0.0	0.0
1	9	12	0.	0.0	0.0
1	10	12	0.	0.0	0.0
1	11	12	0.	0.0	0.0
1	12	12	0.	0.0	0.0
1	13	12	0.	0.0	0.0
1	14	12	0.	0.0	0.0
1	15	12	0.	0.0	0.0
1	16	12	0.	0.0	0.0
1	17	12	0.	0.0	0.0
1	18	12	0.	0.0	0.0
1	19	12	0.	0.0	0.0
1	20	12	0.	0.0	0.0
1	21	12	0.	0.0	0.0
1	22	12	0.	0.0	0.0
1	23	12	0.	0.0	0.0
1	24	12	0.	0.0	0.0
1	25	12	0.	0.0	0.0
1	26	12	0.	0.0	0.0
1	27	12	0.	0.0	0.0
1	28	12	0.	0.0	0.0
1	29	12	0.	0.0	0.0
1	30	12	0.	0.0	0.0
1	31	12	0.	0.0	0.0
1	32	12	0.	0.0	0.0

11

1	1	12	0.	0.0	0.0
1	2	12	0.	0.0	0.0
1	3	12	0.	0.0	0.0
1	4	12	0.	0.0	0.0
1	5	12	0.	0.0	0.0
1	6	12	0.	0.0	0.0
1	7	12	0.	0.0	0.0
1	8	12	0.	0.0	0.0
1	9	12	0.	0.0	0.0
1	10	12	0.	0.0	0.0
1	11	12	0.	0.0	0.0
1	12	12	0.	0.0	0.0
1	13	12	0.	0.0	0.0
1	14	12	0.	0.0	0.0
1	15	12	0.	0.0	0.0

1	16	12	0.	0.0	0.0
1	17	12	0.	0.0	0.0
1	18	12	0.	0.0	0.0
1	19	12	0.	0.0	0.0
1	20	12	0.	0.0	0.0
1	21	12	0.	0.0	0.0
1	22	12	0.	0.0	0.0
1	23	12	0.	0.0	0.0
1	24	12	0.	0.0	0.0
1	25	12	0.	0.0	0.0
1	26	12	0.	0.0	0.0
1	27	12	0.	0.0	0.0
1	28	12	0.	0.0	0.0
1	29	12	0.	0.0	0.0
1	30	12	0.	0.0	0.0
1	31	12	0.	0.0	0.0
1	32	12	0.	0.0	0.0

12

1	1	12	0.	0.0	0.0
1	2	12	0.	0.0	0.0
1	3	12	0.	0.0	0.0
1	4	12	0.	0.0	0.0
1	5	12	0.	0.0	0.0
1	6	12	0.	0.0	0.0
1	7	12	0.	0.0	0.0
1	8	12	0.	0.0	0.0
1	9	12	0.	0.0	0.0
1	10	12	0.	0.0	0.0
1	11	12	0.	0.0	0.0
1	12	12	0.	0.0	0.0
1	13	12	0.	0.0	0.0
1	14	12	0.	0.0	0.0
1	15	12	0.	0.0	0.0
1	16	12	0.	0.0	0.0
1	17	12	0.	0.0	0.0
1	18	12	0.	0.0	0.0
1	19	12	0.	0.0	0.0
1	20	12	0.	0.0	0.0
1	21	12	0.	0.0	0.0
1	22	12	0.	0.0	0.0
1	23	12	0.	0.0	0.0
1	24	12	0.	0.0	0.0
1	25	12	0.	0.0	0.0
1	26	12	0.	0.0	0.0
1	27	12	0.	0.0	0.0
1	28	12	0.	0.0	0.0
1	29	12	0.	0.0	0.0
1	30	12	0.	0.0	0.0
1	31	12	0.	0.0	0.0
1	32	12	0.	0.0	0.0

13

1	1	12	0.	0.0	0.0
1	2	12	0.	0.0	0.0
1	3	12	0.	0.0	0.0
1	4	12	0.	0.0	0.0
1	5	12	0.	0.0	0.0
1	6	12	0.	0.0	0.0
1	7	12	0.	0.0	0.0
1	8	12	0.	0.0	0.0
1	9	12	0.	0.0	0.0
1	10	12	0.	0.0	0.0
1	11	12	0.	0.0	0.0
1	12	12	0.	0.0	0.0
1	13	12	0.	0.0	0.0
1	14	12	0.	0.0	0.0
1	15	12	0.	0.0	0.0
1	16	12	0.	0.0	0.0
1	17	12	0.	0.0	0.0
1	18	12	0.	0.0	0.0
1	19	12	0.	0.0	0.0
1	20	12	0.	0.0	0.0
1	21	12	0.	0.0	0.0
1	22	12	0.	0.0	0.0

1	23	12	0.	0.0	0.0
1	24	12	0.	0.0	0.0
1	25	12	0.	0.0	0.0
1	26	12	0.	0.0	0.0
1	27	12	0.	0.0	0.0
1	28	12	0.	0.0	0.0
1	29	12	0.	0.0	0.0
1	30	12	0.	0.0	0.0
1	31	12	0.	0.0	0.0
1	32	12	0.	0.0	0.0

12

1	1	12	0.	0.0	0.0
1	2	12	0.	0.0	0.0
1	3	12	0.	0.0	0.0
1	4	12	0.	0.0	0.0
1	5	12	0.	0.0	0.0
1	6	12	0.	0.0	0.0
1	7	12	0.	0.0	0.0
1	8	12	0.	0.0	0.0
1	9	12	0.	0.0	0.0
1	10	12	0.	0.0	0.0
1	11	12	0.	0.0	0.0
1	12	12	0.	0.0	0.0
1	13	12	0.	0.0	0.0
1	14	12	0.	0.0	0.0
1	15	12	0.	0.0	0.0
1	16	12	0.	0.0	0.0
1	17	12	0.	0.0	0.0
1	18	12	0.	0.0	0.0
1	19	12	0.	0.0	0.0
1	20	12	0.	0.0	0.0
1	21	12	0.	0.0	0.0
1	22	12	0.	0.0	0.0
1	23	12	0.	0.0	0.0
1	24	12	0.	0.0	0.0
1	25	12	0.	0.0	0.0
1	26	12	0.	0.0	0.0
1	27	12	0.	0.0	0.0
1	28	12	0.	0.0	0.0
1	29	12	0.	0.0	0.0
1	30	12	0.	0.0	0.0
1	31	12	0.	0.0	0.0
1	32	12	0.	0.0	0.0

15

1	1	12	0.	0.0	0.0
1	2	12	0.	0.0	0.0
1	3	12	0.	0.0	0.0
1	4	12	0.	0.0	0.0
1	5	12	0.	0.0	0.0
1	6	12	0.	0.0	0.0
1	7	12	0.	0.0	0.0
1	8	12	0.	0.0	0.0
1	9	12	0.	0.0	0.0
1	10	12	0.	0.0	0.0
1	11	12	0.	0.0	0.0
1	12	12	0.	0.0	0.0
1	13	12	0.	0.0	0.0
1	14	12	0.	0.0	0.0
1	15	12	0.	0.0	0.0
1	16	12	0.	0.0	0.0
1	17	12	0.	0.0	0.0
1	18	12	0.	0.0	0.0
1	19	12	0.	0.0	0.0
1	20	12	0.	0.0	0.0
1	21	12	0.	0.0	0.0
1	22	12	0.	0.0	0.0
1	23	12	0.	0.0	0.0
1	24	12	0.	0.0	0.0
1	25	12	0.	0.0	0.0
1	26	12	0.	0.0	0.0
1	27	12	0.	0.0	0.0
1	28	12	0.	0.0	0.0
1	29	12	0.	0.0	0.0

	1	30	12	0.	0.0	0.0
	1	31	12	0.	0.0	0.0
	1	32	12	0.	0.0	0.0
16						
	1	1	12	0.	0.0	0.0
	1	2	12	0.	0.0	0.0
	1	3	12	0.	0.0	0.0
	1	4	12	0.	0.0	0.0
	1	5	12	0.	0.0	0.0
	1	6	12	0.	0.0	0.0
	1	7	12	0.	0.0	0.0
	1	8	12	0.	0.0	0.0
	1	9	12	0.	0.0	0.0
	1	10	12	0.	0.0	0.0
	1	11	12	0.	0.0	0.0
	1	12	12	0.	0.0	0.0
	1	13	12	0.	0.0	0.0
	1	14	12	0.	0.0	0.0
	1	15	12	0.	0.0	0.0
	1	16	12	0.	0.0	0.0
	1	17	12	0.	0.0	0.0
	1	18	12	0.	0.0	0.0
	1	19	12	0.	0.0	0.0
	1	20	12	0.	0.0	0.0
	1	21	12	0.	0.0	0.0
	1	22	12	0.	0.0	0.0
	1	23	12	0.	0.0	0.0
	1	24	12	0.	0.0	0.0
	1	25	12	0.	0.0	0.0
	1	26	12	0.	0.0	0.0
	1	27	12	0.	0.0	0.0
	1	28	12	0.	0.0	0.0
	1	29	12	0.	0.0	0.0
	1	30	12	0.	0.0	0.0
	1	31	12	0.	0.0	0.0
	1	32	12	0.	0.0	0.0
17						
	1	1	10	0.	25	0.0

```

* Run everything else interactively
Non-interactive grid specification
plane
XYZ
* Coordinate system of output
global
* Output files to create
displacements
elements
strain
* Output file suffix
i400
* Xo, Yo, Zo (Ref.corner), strike,dip,length,width:
0. -500. 0. 0. 90.00 700. 100
* number of grid points in the strike and dip directions (x section 2km grid 700 km NS and 100 km deep)
350 50

```